How Many Electrons Does a Molecular Electride Hold?

Published as part of The Journal of Physical Chemistry virtual special issue "Alexander Boldyrev Festschrift".

Sebastian P. Sitkiewicz, Eloy Ramos-Cordoba,* Josep M. Luis,* and Eduard Matito*

ABSTRACT: Electrides are very peculiar ionic compounds where electrons occupy the anionic positions. In a crystal lattice, these isolated electrons often form channels or surfaces, furnishing electrides with many traits with promising technological applications. Despite their huge potential, thus far, only a few stable electrides have been produced because of the intricate synthesis they entail. Due to the difficulty in assessing the presence of isolated electrons, the characterization of electrides also poses some serious challenges. In fact, their properties are expected to depend on the arrangement of these electrons in the molecule. Among the criteria that we can use to characterize electrides, the presence of a nonnuclear attractor (NNA) of the electron density is both the rarest and the most salient feature. Therefore, a correct description of the NNA is crucial to determine the properties of electrides. In this paper, we analyze the NNA and the surrounding region of nine molecular electrides to determine the number of isolated electrons held in the electride. We have seen that the correct description of a molecular electride hinges on the electronic structure method employed for the analyses. In particular, one should employ a basis set with sufficient flexibility to describe the region close to the NNA and a density functional approximation that does not suffer from large delocalization errors. Finally, we have classified these nine molecular electrides according to the most likely number of electrons that we can find in the NNA. We believe this classification highlights the strength of the electride character and will prove useful in designing new electrides.

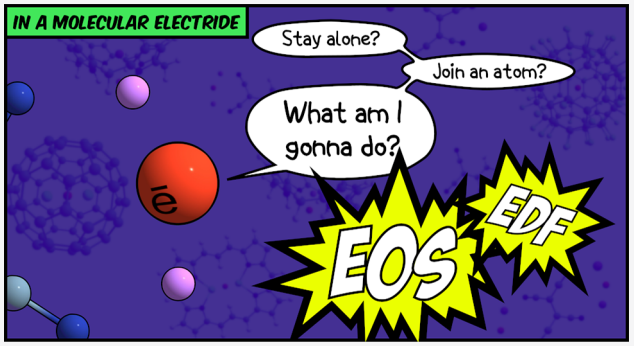

INTRODUCTION

Electrides are ionic species with electrons occupying the anionic positions.[1−4] These anionic electrons in electrides act as separated individual entities, constituting the smallest possible anions in a molecule. All materials present defects at any temperature due to misalignment or absence of atoms, the latter giving rise to vacancies that other particles can occupy. Farbe centers (from the German word *Farbe* = color), commonly known as F centers, are vacancies occupied by electrons randomly placed around the solid. The electrons in the vacancies can undergo energetic excitations (typically in the UV−vis range) that give rise to colors in some mineral crystals such as gemstones. Electrides actually present stoichiometric F centers, i.e., the vacancies and isolated electrons are replicated in the crystal lattice. Electrides resemble alkaline metal solutions of ammonia, which form gold−blue colored materials that consist of positively charge alkaline metals and free electrons solvated by ammonia molecules. An important difference between electrides and solvated electrons is that the latter occur in the liquid disordered state, whereas the electrides have ordered geometrical structures.

James L. Dye, who had been working on the synthesis and characterization of compounds presenting anionic alkali metals—now commonly known as alkalides[5]—was the first who hypothesized the existence of electrides. In 1983, he managed to synthesize the first electride,[6] and, finally, in 1986, he could unequivocally characterize it from the crystallographic structure.[7] Afterward, he also synthesized and characterized other electrides based on alkali metals, but unfortunately, they all eluded thermal stability or air sensitivity.[8,9] The electronic structure of these electrides hinges on the coordination of alkaline cations in a network structure and the formation of cavities (cages or channels) to allocate the isolated electrons. For this reason, cryptand or crown ethers were chosen as complexants. However, all the organic electrides based on cryptand or crown ethers synthesized thus far were not stable at room temperature and spontaneously decomposed at

Table 1. List of Electrides Synthesized up to 2021, Including the Type (Organic/Inorganic), Its Stability at Room Temperature with Respect to Air Exposure (Yes/No), Whether It Is Stable in the Presence of Water and Acid, and the Electron Confinement Regimen (Zero-, One-, and Two-Dimensional or Nanoparticle)

electride	type	stable	confinement	ref
$Cs^+(18C6)_2{\cdot}e^-$	org.	not	1D	6
$K^+(C222){\cdot}e^-$	org.	not	2D	54,55
$Cs^+(15C5)_2{\cdot}e^-$	org.	not	1D	56
$Cs^+[(15C5)(18C6)]_6(18C6)$	org.	not	2D	57
$K^+(15C5)_2{\cdot}e^-$	org.	not	1D	4
$Li^+(C211){\cdot}e^-$	org.	not	1D	58
$Rb^+(C222){\cdot}e^-$	org.	not	1D	59
$C12A7{:}e^-$	inorg.	yes	0D	11
Na^+[tripip-aza(222)]$\cdot e^-$	org.	yes	1D	10
$[Ca_2N]^+{\cdot}e^-$	inorg.	yes	2D	27
$[Y_2C]^{1.8+}{\cdot}1.8e^-$	inorg.	yes	2D	60
$La_8Sr_2(SiO_4)^{64+}{\cdot}4e^-$	inorg.	yes	1D	26
$[Y_5Si_3]^{0.79+}{\cdot}0.79e^-$	inorg.	yes (water)	1D	61
LnH_2 (Ln = La, Ce, Y)	inorg.	yes	0D	22
exfoliated Ca_2N	inorg.	yes	2D	33
Nb_5Ir_3	inorg.	yes	1D	24
Sr_5P_3	inorg.	yes	1D	25
AeAlSi (Ae = Ca, Sr, Ba)	inorg.	yes	2D	30
LaScSi	inorg.	yes	3D	35
$LaCu_{0.67}Si_{1.33}$	inorg.	yes	3D	36
$Ru/C12A7{:}e^-$	inorg.	yes	0D	62
Yb_5Sb_3	inorg.	yes	2D	29
$Ag{-}Ca_2N$	inorg.	yes	2D	63
$LaCu_{0.67}Si_{1.33}$	inorg.	yes	NP	42
Y_5Si_3	inorg.	yes	NP	42
Sr_3CrN_3	inorg.	N/A	1D	23
Y_3Pd_2	inorg.	yes	3D	40
LaRuSi	inorg.	yes	3D	37
LnRuSi (Ln = La, Ce, Pr, Nd)	inorg.	yes (water, acid)	3D	38
LnNiSi (Ln = La, Ce, Pr, Nd)	inorg.	yes	3D	39
Gd_2C	inorg.	yes	2D	28
Hf_2S	inorg.	yes (water, acid)	2D	32
$(Ca_{1-x}Ba_x)12A7{:}e^-$ $(0 \le x \le 0.05)$	inorg.	yes	0D	64
$Sn/C12A7{:}e^-$	inorg.	yes	NP	41
$(C_{1-x}S_x)12A7{:}e^-$ $(0 \le x \le 0.03)$	inorg.	yes	0D	65

temperatures above −40 °C. It actually took quite a long time to design the appropriate ligand (a cryptand[2.2.2]) to retain the cation that, in turn, would trap the electron in a close cavity.[10] The synthesis of complexants that can bind alkali cations is tedious and complicated, and, in this case, it required previous computational calculations that guided the synthesis. Namely, electronic structure calculations suggested that decreasing the electronegativity of the coordination atom by replacing oxygen with nitrogen would raise the complexants' LUMO energies enough to make them inaccessible for the electron attachment that leads to the thermal decomposition of these complexants.[10]

Although Dye synthesized the first stable *organic* electride in 2005, the first stable electride was discovered by the group of Hideo Hosono 2 years earlier.[11] $[Ca_{24}Al_{28}O_{64}]^{4+}(4e^-)$ is an inorganic electride that has found many applications: an electron emitter,[12] an electron injection electrode for organic semiconductors,[13] a synthetic organic reagent in pinacol coupling reaction,[14] a cathode in top-emission organic light-emitting diodes,[15] a reversible H_2 storage device,[16] a catalyst in the synthesis of ammonia,[17] an electrode in electrochemical reactions,[18] fabrication of a field-effect transistor,[19] as a cathode in a fluorescent lamp,[20] and an electric conductor.[21] The group of Hosono has been the most active in the search for new (inorganic) electrides with appealing applications, but other groups have recently joined the quest. Nowadays, there is a large collection of electrides, which can be classified according to the shape of the lattice voids where electrons are trapped: zero-dimensional electrides,[22] one-dimensional electrides,[23−26] two-dimensional electrides,[27−34] three-dimensional ones,[35−40] and electride nanoparticles.[41,42] In Table 1, we have collected all the experimental realizations of electrides, indicating which of them are stable at room temperature, whether they are organic or inorganic, and the number of dimensions of the isolated electron cavity. There are, however, other electrides that have been suggested in the literature based on computational calculations.[43,44] This is the case of *molecular electrides*,[45] which are single-molecule electrides, or metal cluster electrides,[46] in which a sea of delocalized valence electrons surround the metal cation.

Another route to design electrides avoiding chelating organic molecules consists in applying high pressures (hundreds of GPa) to alkaline metal structures.[47] Upon compression of valence electrons, they separate one from another to minimize

the electron repulsion. This way, there is a greater difficulty for electrons to move freely in the lattice, and the material becomes a Mott insulator. This behavior has been observed in Li,[48] Na,[49] K,[47] and Mg.[50] These compounds were characterized by non-nuclear attractors (NNA) and maxima of the electron localization function (ELF),[51] with a large number of electrons (between 1 and 2) in the corresponding basins. Hoffmann has worked on the chemical bonding formed between electrons of high-pressure electrides (called interstitial quasi-atoms (ISQs)) and their bonding capabilities, which can be traced back to those of atomic clusters in the so-called *superatoms*.[52,53] An ISQ does not contain nuclei or core electrons, yet due to its space confinement, an ISQ in a high-pressure electride acts as a regular atom, accommodating electrons and forming anions, giving rise to covalent and metallic bonds with the neighboring ISQs or atoms. Therefore, ISQs can form *quasimolecules* such as E_2 bonds, LiE, MgE_2, and EB, among others; E being the electron at the ISQ.

The characterization of electrides is not free of ambiguity.[45,46,66] Nevertheless, electrides present several special properties that could be used to identify them. For instance, solid-state electrides show particular magnetic features that result from the presence of unpaired spins, such as exalted susceptibilities that correlate with the area of the channel where the isolated electrons are located. An electride is expected to be a Mott insulator, and some electrides are superconductors at low temperatures.[13,67−69] In addition, they also present huge nonlinear optical properties (NLOPs), which include some of the largest static first hyperpolarizabilities ever reported.[70,71] However, none of these properties are exclusive of electrides, and one is deemed to measure the most salient feature of electrides: the existence of an isolated electron. Hence, the characterization of electrides depends on experimental and computational techniques that can unequivocally identify the presence of isolated electrons. Since the density of free electrons is not large enough to be located in the X-ray of the crystal structure, most experimental evidence of the presence of this electron is indirect[8,9,72] and comes usually from (i) the similarity of the electride structure with analog alkalides (i.e., the cationic structure), (ii) the chemical shift of the corresponding cation, (iii) EPR studies, and (iv) atomic-resolution scanning tunneling microscopy.[73] The theoretical analysis often provides more reliable ways to characterize electrides, e.g., through the characterization of the topology of the electron density, the ELF,[51,74,75] the noncovalent interactions (NCI),[76,77] the localized-orbital locator (LOL),[78] and the Laplacian of the electron density.[79] These tools are useful to identify localized electrons in electrides[45,46,66,80] but these features are also separately present in many systems that cannot be considered electrides. In 2015, some of us established the following computational criteria to identify molecular electrides: the presence of an NNA, a highly localized density (indicated by the ELF, the Laplacian of the electron density, or another indicator such as LOL), and large nonlinear optical properties.[45] Dale et al. have recently also reviewed these and other criteria to recognize electrides.[66] They confirm that our criteria are adequate to identify molecular electrides; however, they found some difficulties in detecting NNAs in inorganic electrides because of the compact nature of their vacancies.[66] One should also keep in mind that many density functional approximations (DFAs) suffer from delocalization errors caused by spurious self-interactions (known as the self-interaction error) that result in the overestimation of the electron delocalization in the molecule.[81] As a result, DFAs with a low percentage of Hartree−Fock (HF) exchange tend to overestimate electron conjugation[82] and aromaticity.[83−86] In the case of electrides, the delocalization error might hinder the presence of NNAs in electronic densities of solid-state inorganic electrides (*vide infra*).[80]

Among the criteria that can be used to identify electrides, the NNA is the rarest feature. Therefore, it is assumed that the existence of an NNA indicates that, most likely, the molecule is an electride. It is thus important to find the suitable electronic structure method to detect the NNA, which, as we shall see, is quite sensitive to both the accuracy of the method and the quality of the basis set employed. The correct characterization of the electron density around the NNA is necessary to assess the properties of the NNA basin (delimited by the density zero-flux surface surrounding the NNA), which, in turn, will determine the properties of the electride. In this sense, some questions about electrides remain unanswered. Which is the most likely number of electrons that holds an electride? Can we connect the latter with the formal *oxidation state* of the NNA basin? Which is the probability of finding at least one electron in the NNA basin? To which extent are the isolated electrons in an electride localized? In this paper, we will address these queries and show a few types of electrides according to the number of electrons the NNA basin holds. We will also assess the sensitivity of the computational method employed to characterize molecular electrides. We believe this study, apart from providing insight on the formal characterization of the electrides, will also help to understand the electronic structure arrangement in molecular electrides and, therefore, help in the design of new electrides.

METHODOLOGY

In this paper, we have studied several molecules (see Figure 1 for the molecular representation of the systems) that were already classified as molecular electrides following the criteria we established:[45] Li@calix[4]pyrrole,[45,70,87] Na@calix[4]-pyrrole,[88] $TCNQLi_2$,[45,89] $TCNQNa_2$,[45,89] $TCNENa_3$,[90] $TCNENa_4$(II),[90] Mg_2EP,[91] $Mg_2@C_{60}$,[88] and $e@C_{60}F_{60}$.[45,92] Namely, all of these systems present at least an NNA, a highly localized density in the region of the NNA—indicated by the large negative value of the Laplacian of the electron density[79] or the presence of an ELF[51,74] basin—and large nonlinear optical properties (NLOPs). For $TCNENa_3$ and $TCNENa_4$(II), only the values of the static first hyperpolarizability were reported.[90] For the sake of completeness, in the Supporting Information, we have included the static NLOPs of these molecules (up to the second hyperpolarizability), which are of the same magnitude as in other molecular electrides.

All structures were optimized at the CAM-B3LYP/ma-TZVP[93,94] level of theory. It has been recently documented that this functional avoids large delocalization errors,[83−85] which could give rise to spurious critical points in the potential energy surface.[86,95] For these optimized geometries, single-point calculations with various basis sets and density functional approximations (CAM-B3LYP,[93] B3LYP,[96,97] M06-2X,[98] and MN15[99]) as well as Hartree−Fock (HF) and MP2[100] methods have been performed. Although HF completely neglects electron correlation and, in most cases, density functional approximations (DFAs) provide more accurate energies and geometries, DFAs struggle to reproduce the electron density of some electrides with unpaired electrons. Conversely, HF

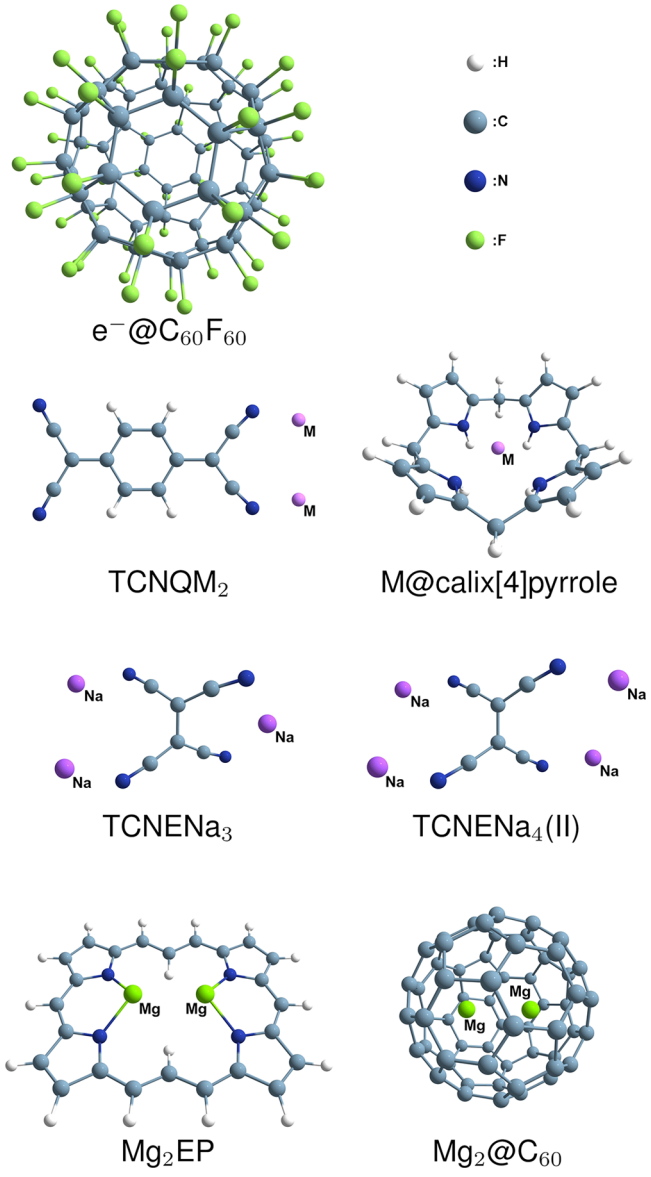

Figure 1. Molecular representations of Li@calix[4]pyrrole,[45,70,87] Na@calix[4]pyrrole,[88] $TCNQLi_2$,[45,89] $TCNQNa_2$,[45,89] $TCNENa_3$,[90] $TCNENa_4$(II),[90] Mg_2EP,[91] $Mg_2@C_{60}$,[88] and $e@C_{60}F_{60}$[45,92] optimized at the CAM-B3LYP/ma-TZVP level of theory. Molecules with an M atom have been optimized and studied for M = Li and M = Na.

densities are usually of sufficient quality (at least they do not suffer from delocalization errors) to provide a correct description of the system. This way, we have an alternative method that, in some cases, provides results closer to correlated *ab initio* methods (see Results). The purpose of performing such benchmarking calculations is to assess the accuracy of each DFA and measure the effect of the delocalization error in the characterization of the isolated electron(s). For $TCNENa_3$, additional calculations with CCSD and CCSD(T) were also included to assess the performance of MP2, which is the reference for all the other systems. In order to confirm the single-reference nature of $TCNENa_3$, we performed T1[101] and D1 diagnostics[102] on the coupled-cluster wave function. For all CCSD and MP2 wave functions, we have computed the I_{ND} index[103,104] obtained from the range-separation partition of the Coulomb hole.[105,106] I_{ND} is proportional to the deviation from idempotency of the first-order reduced density matrix.[107,108] Unlike T1 and D1 diagnostics, I_{ND} can be calculated for any wave function from natural orbital occupations. All HF, MP2, and DFAs calculations were performed with Gaussian16 (Rev. B01),[109] whereas CCSD and CCSD(T) calculations were computed using CFOUR 2.1.[110] For all post-HF methods, relaxed one-electron densities[111] have been employed in the subsequent analyses, whereas the Muller approximation[112] has been employed to compute approximate two-electron densities from natural orbital occupancies.[113,114] The latter are used to calculate the localization index and the probabilities (*vide infra*). Such an approach has been used in the past to calculate reasonably accurate localization and delocalization indices.[113,115−119]

The study of the electronic distribution in electrides was done in the framework of the quantum theory of atoms in molecules (QTAIM)[79] using the AIMAll package (ver. 19.10.12).[120] This software was used to perform a topological analysis of the electron density, detect the presence of non-nuclear attractors (NNAs),[121] and integrate the number of electrons in the corresponding NNA basins (NNA population). We also calculate the localization index,[118,122] which gives a measure of the number of electrons localized in this region. In addition, we performed an effective oxidation state (EOS) analysis[123,124] to assign an integer number of electrons to the NNA basin. Unlike the NNA population, which gives the average number of electrons in the NNA basin, the NNA EOS is an integer number (or, occasionally, a rational number) expected to provide a value close to the formal *ionic picture*[124] of the NNA basin. The two values provide important complementary information about the electronic structure of a molecule. In order to perform the EOS analysis, we always define one fragment for each NNA basin we have identified in the molecule. The rest of the molecule will be divided into two different ways: (1) considering one whole fragment or (2) separating metallic centers from the rest of the molecule. The EOS method defines a set of effective atomic orbitals (EffAOs) and occupations from the atomic overlap matrix obtained from the QTAIM analysis. The EffAOs are ranked in decreasing occupation order, and one by one, the electrons of the molecule are assigned to the different fragments. The procedure is done separately for α and β electrons. The number of electrons assigned to each fragment determines its oxidation state. At the same time, the occupations of the EffAOs are used to calculate a measure of the uncertainty of the oxidation state assignment (*vide infra*). The EOS analysis has been recently used to assign oxidation states in many nontrivial molecules.[95,125−129] In this work, we have employed APOST3D (dev. ver. 2.0) to perform the EOS study.[130] Finally, we have calculated the electron distribution functions (EDFs)[131] to analyze the probability of finding zero, one, and two electrons in the NNA. To this end, we have implemented the formulation of Cancés et al.[132] in an in-house version of APOST3D.

RESULTS

This section will present the results gathered for the nine molecular electrides we have selected for our study. First of all, we will choose the most suitable computational method to analyze these systems by examining several density functional approximations (DFAs) and *ab initio* methods. Afterward, we will determine the most likely number of electrons that contribute to the electride character of each molecule and

determine the oxidation state of the region that contains the isolated electrons of the studied electrides. Finally, we will compare the different descriptors used to characterize the electrides and determine which ones can assess the number of electrons in electrides.

Calibration of the Computational Method. In this work, we will employ MP2 as the reference method to compare the features obtained from the topological analysis of the electron density, including the density and its Laplacian at the NNA, the average number of electrons in the NNA (N_{NNA}), and the number of electrons localized in the NNA (λ_{NNA}) or localization index.[118,122] In order to assess the accuracy of MP2, we have selected $TCNENa_3$, for which MP2 presented a large deviation for all the DFAs tested (compare N_{NNA} and λ_{NNA} for $TCNENa_3$, *vide infra*), and performed additional CCSD and CCSD(T) calculations. For the sake of convenience, for this particular test, we have selected a smaller basis set, cc-pVTZ, which does not include diffuse functions. Fortunately, for this system, diffuse functions are not needed to obtain accurate descriptors related to the electron density (compare the cc-pVTZ and aug-cc-pVTZ results of Table 2 and the corresponding table for $TCNENa_3$, *vide infra*).

Results of the QTAIM analysis at different levels of theory are displayed in Table 2. MP2 gives essentially the same topology of the density as CCSD and CCSD(T), including the value of the density and its Laplacian at the position of the NNA. The average number and the localized electrons in the NNA basin are very similar for MP2, CCSD, and CCSD(T) wave functions and slightly overestimated using a HF wave function. In order to assess the single-reference character of this system, we performed T1 and D1 diagnostics, which confirmed the lack of multireference character in this system (see Table 3). Further confirmation is obtained from the largest single and double excitation amplitudes in CCSD, which are of the order of 0.02. Finally, in Table 4, we collect I_{ND} for all the MP2 wave functions, which is below 0.037 in all cases, indicating a low multireference character for the molecules studied in this paper (as a reference, I_{ND} = 0.50 for the dissociated H_2 molecule, whereas I_{ND} = 0.038 would correspond to the H_2 molecule at R_{HH} = 0.86 Å, R_{HH} = 0.74 Å being the equilibrium geometry). These results confirm that MP2 is a good reference system to study the electronic distribution in these molecular electrides.

Which Is the Most Likely Number of Electrons in Molecular Electrides? In order to determine the number of electrons in the NNA basin (hereafter, electron numbers), we analyze several properties related to the NNA. First, we collect some topological indicators such as the electron density at the non-nuclear attractor, $\rho(\mathbf{r}_{NNA})$, and the local charge concentration at this point, measured through the Laplacian of the electron density, $\nabla^2\rho(\mathbf{r}_{NNA})$. We expect these quantities to increase and decrease, respectively, with the electron numbers.

Table 2. Results of the QTAIM Partitioning for $TCNENa_3$ at Various Levels of Theory with the cc-pVTZ Basis Set[a]

method	$\rho(\mathbf{r}_{NNA})$	$\nabla^2\rho(\mathbf{r}_{NNA})$	N_{NNA}	λ_{NNA}
HF	7.2×10^{-3}	-5.4×10^{-3}	0.487	0.231
MP2	7.1×10^{-3}	-5.3×10^{-3}	0.459	0.206
CCSD	7.1×10^{-3}	-5.3×10^{-3}	0.459	0.207
CCSD(T)	7.1×10^{-3}	-5.2×10^{-3}	0.453	0.202

[a]For the description of columns, see Table 5.

Table 3. Multireference Diagnostics of the $TCNENa_3$ CCSD Wavefunction with Different Basis Sets[a]

basis set	T_1	D_1	I_{ND}
cc-pVTZ	0.0164	0.0446	0.022
def2-TZVP	0.0164	0.0448	0.022

[a]All the calculations display values below the recommended thresholds ($T_1^{MR} \geq 0.02$ and $D_1^{MR} \geq 0.05$).[101,102]

Table 4. Values of the Nondynamical Correlation Index (I_{ND})[103,104] Calculated Using Occupancies of Natural Orbitals Obtained with MP2 and Various Basis Sets

molecule	basis set	I_{ND}
$TCNQLi_2$	aug-cc-pVTZ	0.021
	ma-TZVP	0.021
$TCNQNa_2$	aug-cc-pVTZ	0.019
	ma-TZVP	0.018
Li@calix[4]pyrrole	aug-cc-pVTZ	0.030
	ma-TZVP	0.029
Na@calix[4]pyrrole	aug-cc-pVTZ	0.029
	ma-TZVP	0.028
$TCNENa_3$	aug-cc-pVTZ	0.023
	ma-TZVP	0.023
$TCNENa_4$(II)	aug-cc-pVTZ	0.020
	ma-TZVP	0.020
Mg_2EP	aug-cc-pVTZ	0.031
	ma-TZVP	0.031
$Mg_2@C_{60}$	aug-cc-pVTZ	0.036
	ma-TZVP	0.036
$e@C_{60}F_{60}$	6-31G(d)+DF	0.021
	6-31+G+DF	0.017
	6-31G+DF	0.017
	cc-pVDZ+DF	0.021

We also measure the average number of electrons that we can find in the NNA basin, N_{NNA}, and the number of localized electrons in this basin, λ_{NNA}. The latter quantity is directly connected with the uncertainty in the electron population of the NNA basin, δ_{NNA}, where $N_{NNA} = \lambda_{NNA} + \delta_{NNA}$.[118,133,134]

We also compute the probability of having exactly zero, one, and two electrons inside the NNA basin for single-determinant wave functions (in the case of DFAs, we employ the Kohn–Sham wave function and, hence, it should be considered as an approximation to the actual probabilities provided by the corresponding DFA), which following the work of Cancés et al.,[132] can be calculated as follows:

$$P_0^A = \prod_{i=1}^{N} (1 - \lambda_i^A) \tag{1}$$

If $P_0^A \neq 0$, the probability of finding exactly n electrons in the region A, P_n^A, is given by

$$P_n^A = \sum_{i_1,\ldots,i_n}{}' \prod_{j=1}^{n} \left(\frac{\lambda_{i_j}^A}{1 - \lambda_{i_j}^A} \right) P_0^A \;\forall \quad n > 0 \tag{2}$$

where the prime in the summation indicates that we are excluding terms with repeated indices, and λ_i^A are the N eigenvalues of the atomic overlap matrix for the basin A. Hereafter, we only consider the basin of the NNA and thus we drop the notation indicating the region ($P_i \equiv P_i^{NAA}$ and $\lambda_i \equiv \lambda_i^{NNA}$). These probabilities, which are now generically known as

Table 5. Results of the QTAIM Partitioning for $TCNQLi_2$[a]

method	basis	$\rho(\mathbf{r}_{NNA})$	$\nabla^2\rho(\mathbf{r}_{NNA})$	N_{NNA}	λ_{NNA}	EOS[1]	RI	EOS[2]	RI	P_0	P_1	P_2
CAM-B3LYP	ma-TZVP					no NNAs						
	ma-QZVP	9.6×10^{-3}	-8.2×10^{-3}	0.540	0.277	−1	55	−1	83	46.9	52.6	0.6
	cc-pVTZ	9.6×10^{-3}	-8.3×10^{-3}	0.563	0.300	−1	60	−1	87	44.7	54.7	0.6
	aug-cc-pVTZ	9.6×10^{-3}	-8.3×10^{-3}	0.557	0.295	−1	59	−1	86	45.2	54.2	0.6
B3LYP	ma-TZVP					no NNAs						
	ma-QZVP	9.4×10^{-3}	-7.9×10^{-3}	0.505	0.242	0	52	−1	79	50.3	49.2	0.5
	cc-pVTZ	9.4×10^{-3}	-8.1×10^{-3}	0.527	0.262	−1	52	−1	82	48.3	51.2	0.6
	aug-cc-pVTZ	9.4×10^{-3}	-8.1×10^{-3}	0.524	0.259	−1	52	−1	81	48.5	50.9	0.6
M06-2X	ma-TZVP[b]	7.8×10^{-3}	-4.5×10^{-3}	0.424	0.084	0	68	−1	67	58.3	41.2	0.5
	ma-QZVP	9.3×10^{-3}	-7.9×10^{-3}	0.607	0.344	−1	67	−1	94	40.6	58.4	1.0
	cc-pVTZ	9.4×10^{-3}	-8.3×10^{-3}	0.609	0.345	−1	67	−1	94	40.6	58.4	1.1
	aug-cc-pVTZ	9.5×10^{-3}	-8.3×10^{-3}	0.609	0.346	−1	68	−1	94	40.5	58.5	1.0
HF	ma-TZVP	7.8×10^{-3}	-4.7×10^{-3}	0.593	0.337	−1	66	−1	90	41.5	57.9	0.6
	ma-QZVP	9.6×10^{-3}	-8.5×10^{-3}	0.726	0.504	−1	92	−1	100	28.7	70.5	0.9
	cc-pVTZ	9.7×10^{-3}	-8.7×10^{-3}	0.719	0.494	−1	91	−1	100	29.4	69.8	0.8
	aug-cc-pVTZ	9.7×10^{-3}	-8.7×10^{-3}	0.724	0.502	−1	92	−1	100	28.8	70.3	0.9
MP2	ma-TZVP	8.0×10^{-3}	-4.8×10^{-3}	0.550	0.291					45.6	53.9	0.6
	aug-cc-pVTZ	1.0×10^{-2}	-9.1×10^{-3}	0.700	0.470					31.0	68.0	1.0

[a]The third and fourth columns report values of the density, $\rho(\mathbf{r}_{NNA})$, and its Laplacian, $\nabla^2\rho(\mathbf{r}_{NNA})$, at the positions of the NNA. The fifth and sixth columns give the population, N_{NNA}, and localization index, λ_{NNA}, for the NNA basin. Starting on the seventh column, results of the EOS and EDF analyses of the NNA basin are given. EOS[1] and EOS[2] correspond to the oxidation state obtained with type 1 and 2 fragmentations, respectively (see text). The last three columns report the probabilities (in percentage) of finding 0, 1, and 2 electrons in the NNA basin. [b]Two closely separated NNAs are found for this basis set (N_{NNA} and λ_{NNA} correspond to the sum of both NNAs).

electron distribution functions (EDFs), were introduced in chemistry by Daudel[135,136] and have been extensively used by Pendás and co-workers[131,137,138] as an elegant tool to characterize chemical bonds.[139] One can easily retrieve the average number of electrons in the NNA basin using the EDFs:

$$N_{NNA} = \sum_i iP_i \tag{3}$$

In the present case, the probability of finding more than two electrons in the NNA basin is expected to be negligible, hence, $N_{NNA} \approx P_1 + 2P_2$. Despite MP2 probabilities cannot be computed from eqs 1 and 2, neglecting P_i $\forall i > 2$, and employing the approximate localization index (*vide supra*), we can compute approximate MP2 P_0, P_1, and P_2 from the following set of equations:

$$N_{NNA} \approx P_1 + 2P_2 \tag{4}$$

$$\lambda_{NNA} \approx N_{NNA} - P_0(N_{NNA})^2 - P_1(1 - N_{NNA})^2 - P_2(2 - N_{NNA})^2 \tag{5}$$

$$1 \approx P_0 + P_1 + P_2 \tag{6}$$

which give rise to these approximate probabilities:

$$P_0 \approx 1 - N_{NNA} + \frac{1}{2}({N_{NNA}}^2 - \lambda_{NNA}) \tag{7}$$

$$P_1 \approx \lambda_{NNA} + N_{NNA}(1 - N_{NNA}) \tag{8}$$

$$P_2 \approx \frac{1}{2}({N_{NNA}}^2 - \lambda_{NNA}) \tag{9}$$

Obviously, if $P_i \approx 0$ $\forall i > 2$ and for accurate N_{NNA} and λ_{NNA}, the latter expressions provide excellent estimates of eqs 1 and 2 regardless of the wave function approximation. We consider that the molecule is at least a one-electron molecular electride if the probability of having at least one electron, $1 - P_0$, is higher than the opposite, P_0.

Finally, we employ the effective oxidation state (EOS) tool developed by Salvador and co-workers.[123,124] Namely, we calculate the EOS of the NNA basin. To compute the EOS, we must define real-space fragments among which the electrons are distributed. We test two partitions: EOS[1], which considers only two fragments, the NNA basin and the rest of the molecule, and EOS[2], which divides the space into several fragments, the NNA basins, one fragment for each metallic atom, and the rest of the molecule. The only exception is the $e@C_{60}F_{60}$ system, in which only type 1 fragmentation can be applied because there are no metallic centers. The reliability index (RI) is a measure that accompanies the EOS analysis, giving the likelihood of a correct prediction of the oxidation state. The RI is calculated using the following expression:

$$\mathrm{RI}(\%) = 100 \min(R_\alpha, R_\beta) \tag{10}$$

where

$$R_\sigma = \min(1, \Delta\lambda^\sigma + 1/2) \tag{11}$$

and $\Delta\lambda^\sigma = \lambda^\sigma_{LO} - \lambda^\sigma_{FU}$, LO and FU staying for lowest-occupied and first-unoccupied EffAOs, respectively. RI takes values between 50% (highest uncertainty) and 100% (lowest uncertainty). The EOS will be compared against the highest P_i value obtained from the EDFs.

$TCNQLi_2$. The ground state of $TCNQLi_2$ ($^3B_1$) was characterized using different methods and various basis sets (see Table 5). In all cases, except for B3LYP/ma-TZVP, CAM-B3LYP/ma-TZVP, and M06-2X/ma-TZVP densities, a single non-nuclear attractor was located between the Li atoms (see Figure 2). B3LYP/ma-TZVP and CAM-B3LYP/ma-TZVP electronic densities do not display an NNA whereas, in the case of M06-2X/ma-TZVP, two close NNAs are located between Li atoms. Except for the calculations performed with the ma-TZVP basis set,[94] the density and its Laplacian values at the NNA are very similar for all the methods and basis sets studied. A careful inspection of this basis set reveals that ma-

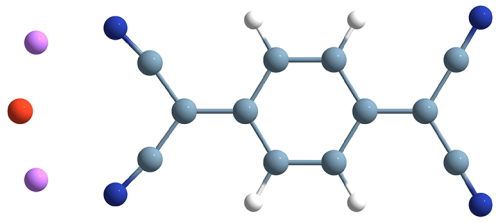

Figure 2. Geometry of $TCNQLi_2$ optimized at the CAM-B3LYP/ma-TZVP level of theory. A single-point calculation with the aug-cc-pVTZ basis set was used to retrieve the position of the NNA, which is indicated with a red ball.

TZVP does not present functions of angular momentum higher than 1 for Li, whereas ma-QZVP, cc-pVTZ, and aug-cc-pVTZ present d and f functions and some extra p functions with lower exponents. Since we are employing atom-centered basis sets, the presence of the latter functions on Li is essential for a correct description of the electron density in the NNA region. For this reason, we will not consider the results obtained with the ma-TZVP basis set for this molecule.

The population and the number of electrons localized at the NNA basin increase with the percentage of HF exchange employed in the method (B3LYP, 20%, CAM-B3LYP, 19–65%, M06-2X, 54%, HF, and MP2, 100%), HF providing the closest agreement with MP2 data. The population of the NNA oscillates between 0.5 and 0.7 electrons, in agreement with the oxidation state of −1 assigned by the EOS analysis. This oxidation state is predicted with a RI that increases with the average number of electrons and the number of electrons localized in the NNA (compare different methods in Table 5). Interestingly, the RI increases if the electrons are distributed among more fragments. Namely, the RI is larger for EOS[2], which distributes the electrons in the electrides among the NNA, the two Li atoms, and the rest of the molecule. As we shall see, it is not the most common situation; more fragmentation usually increases the uncertainty of the EOS assignment, and in general, EOS[1] will be equal to or higher than EOS[2]. A simple inspection of the probability distributions in the NNA basin reveals that the highest probability always corresponds to the oxidation state predicted by the EOS analysis. Furthermore, there is a good correspondence between the value of the probability and the RI value predicted by the first fragmentation (EOS[1]). In this case, the two most likely events are those in which the NNA basin holds zero and one electron, the latter being clearly the preferred situation for most methods. Hence, according to EOS and EDF criteria, we can classify $TCNQLi_2$ as a one-electron molecular electride.

$TCNQNa_2$. The results of the ground state of $TCNQNa_2$ ($^3B_1$) are collected in Table 6 (see also Figure 3). In this case, the ma-TZVP basis set of sodium contains some d and some extra p functions with lower exponents, which help describe the NNAs. However, these extra basis functions are insufficient to provide a description that matches the results obtained with the aug-cc-pVTZ basis set. The values of the density and its Laplacian at the NNA are very similar with both basis sets, but the population and, especially, the localization index are more sensitive to the quality of the basis set.

As compared to $TCNQLi_2$, $TCNQNa_2$ has lower electron numbers and less localized electrons in the NNA. More than 50% of the electrons in the NNA basin were localized in the former case, whereas for $TCNQNa_2$ this number is about 25% for the studied DFAs and below 50% for HF and MP2. In fact, regardless of the method or basis set employed in the calculation, the probability of finding no electron in the NNA basin is clearly larger than the probability of having one or more electrons. For this molecule, the topological features obtained with the MP2 wave function are much closer to the values obtained at the HF level of theory, suggesting that all DFAs underestimate the electride character of this molecule. According to MP2, the probability of having one or more electrons is 46%, which is quite high. This result is in line with the EOS analysis at the same level of theory, which attributes different oxidation states, 0 or −1, depending on the number of fragments used. In this sense, this molecule is a borderline situation between a zero-electron and a one-electron molecular electride.

Li@calix[4]pyrrole and Na@calix[4]pyrrole. The results of the ground state of Li@calix[4]pyrrole[45,70,87] ($^2A_1$) and Na@calix[4]pyrrole[45,87] ($^2A_1$) are collected in Tables 7 and 8, respectively (see also Figure 4). Unlike $TCNQLi_2$, in this case, ma-TZVP provides qualitatively similar results to aug-cc-pVTZ because the Li and N atoms are closer to the NNA. Therefore, the p functions centered in Li (as well as the diffuse functions in the neighboring N atoms) provide a better description of the NNA.

CAM-B3LYP density descriptors are clearly closer to the MP2 ones, and hence we will focus on the EOS and EDF analyses at the CAM-B3LYP/aug-cc-pVTZ level of theory. The average population and the localized electrons of the NNA basin are rather low, in agreement with the zero oxidation state and the high RI assigned by the EOS analysis. The EDF analysis confirms that the probability of having zero electrons

Table 6. Results of the QTAIM Partitioning, EOS, and EDF Analyses for $TCNQNa_2$[a]

method	basis	$\rho(\mathbf{r}_{NNA})$	$\nabla^2\rho(\mathbf{r}_{NNA})$	N_{NNA}	λ_{NNA}	EOS[1]	RI	EOS[2]	RI	P_0	P_1	P_2
CAM-B3LYP	ma-TZVP	6.9×10^{-3}	-4.4×10^{-3}	0.213	0.044	0	100	0	66	78.9	21.0	0.0
	aug-cc-pVTZ	7.1×10^{-3}	-4.9×10^{-3}	0.265	0.068	0	98	0	58	73.7	26.2	0.1
B3LYP	ma-TZVP	6.6×10^{-3}	-4.1×10^{-3}	0.170	0.028	0	100	0	72	83.2	16.8	0.0
	aug-cc-pVTZ	6.8×10^{-3}	-4.6×10^{-3}	0.217	0.045	0	100	0	65	78.6	21.3	0.0
M06-2X	ma-TZVP	6.7×10^{-3}	-4.0×10^{-3}	0.236	0.053	0	100	0	62	76.7	23.2	0.1
	aug-cc-pVTZ	6.9×10^{-3}	-4.5×10^{-3}	0.241	0.054	0	100	0	61	76.3	23.6	0.1
HF	ma-TZVP	7.1×10^{-3}	-5.2×10^{-3}	0.443	0.191	0	63	−1	68	56.2	43.7	0.2
	aug-cc-pVTZ	7.1×10^{-3}	-5.4×10^{-3}	0.495	0.238	0	52	−1	75	51.0	48.8	0.2
MP2	ma-TZVP	7.3×10^{-3}	-5.3×10^{-3}	0.418	0.171					58.4	41.4	0.2
	aug-cc-pVTZ	7.4×10^{-3}	-5.6×10^{-3}	0.465	0.212					53.7	46.0	0.2

[a]For a full description, see Table 5.

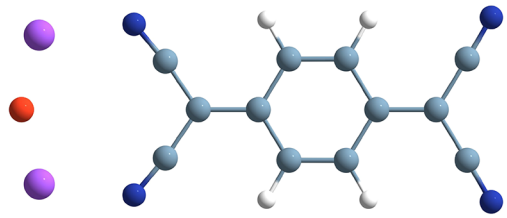

Figure 3. Geometry of $TCNQNa_2$ optimized at the CAM-B3LYP/ma-TZVP level of theory. The NNA position is indicated with a red ball.

in the NNA basin is the largest one. However, it also reveals a non-negligible probability of 26.3% and 16.5% (28.8% and 19.5% at the MP2 level) of having one or more electrons in the NNA basin of Li@calix[4]pyrrole and Na@calix[4]pyrrole, respectively. Both molecules can be thus classified as low-electron-number electrides.

$TCNENa_3$ and $TCNENa_4$(II). The results for the ground state of $TCNENa_3$ (^2A) and $TCNENa_4$(II) ($^3B_3$) are collected in Tables 9 and 10, respectively. Both compounds were recently classified as molecular electrides.[90] The former presents a Na−Na pair between which we can locate an NNA, whereas the latter has two Na−Na pairs, giving rise to two symmetrically equivalent NNAs (see Figure 5). In this case, we will discuss the HF results because they provide the best agreement with the MP2 data. According to the topological analysis of the electron density, the oxidation state analysis, and electron distribution functions, both molecules have qualitatively the same electride character of $TCNQNa_2$; i.e., they can be considered borderline situations between zero- and one-electron molecular electrides.

Mg_2EP. The results of the ground state of Mg_2EP ($^1A_1$) are collected in Table 11. This molecule was classified as a molecular electride by Chattaraj and co-workers,[91] and it displays an NNA between the two Mg atoms (see Figure 6). In this case, all density functional approximations give very similar values, and MP2 results lie in between HF and CAM-B3LYP values. The average number of electrons in the NNA basin is quite large compared to previous molecules. The EOS analysis assigns two different oxidation states, 0 or −2, depending on the partition scheme. Due to the spin symmetry of the molecule (this is a closed-shell system), the EOS cannot assign an oxidation state of −1 to the NNA basin. The electron distribution analysis reveals an important difference with previous molecules: the probability of having two electrons in the NNA is not negligible and ranges between 11 and 25% depending on the level of theory. As we shall discuss later, this feature will be important to compare the EOS and EDF analyses. Interestingly, regardless of the methodology employed in the calculation, the probability of having more than one electron at the NNA is always higher than 50%, and the most likely situation is that of having only one electron at the NNA. In this case, there is an obvious disagreement between EOS and EDF, regardless of the partition employed in the former analysis. Still, we can speculate that this molecule is at least a one-electron electride.

$Mg_2@C_{60}$. The results for the ground state of $Mg_2@C_{60}$ (^1A_g) are collected in Table 12. This molecule was also classified as a molecular electride by Chattaraj and co-workers[88] because, among other properties,[45] it presents an NNA between both Mg atoms (see Figure 7). In this case, all density functional approximations provide very similar results to MP2, whereas HF clearly overestimates the electride character of the molecule. The EOS analysis suggests the oxidation state of the NNA is either 0 or −2, depending on the partition employed. The EOS analysis also discards the oxidation state of −1 due to the spin symmetry of the molecule. On the other hand, the probability of finding at least one electron at the NNA basin is larger (56−59% depending on the DFA) than the probability of finding no electron, and the probability of finding exactly two electrons is not negligible (11−13%). The situation in which we have only one electron is the most likely scenario if one has to choose among the three possibilities, although, according to the EDF analysis, no possibility can be ruled out. Hence, we are deemed to conclude that $Mg_2@C_{60}$ is at least a one-electron electride.

***e*@$C_{60}F_{60}$.** Finally, we study the ground state of $e@C_{60}F_{60}$ (^2A_g), which was previously assigned a weak electride character.[45] The results are collected in Table 13. This is the largest molecule studied in this paper and its size prevents the use of large basis sets. One can identify an NNA in the middle of the fullerene cage (see Figure 8). Following previous studies,[45,92] we have augmented medium-sized basis sets with some additional functions placed at the center of the cage to provide a good description of the NNA. Namely, we have added four uncontracted diffuse functions of s- and p-types with exponents $1.68714478 \times 10^{-n}$ ($n = 1-4$). These basis sets have been labeled as +DF (see Table 13). For this molecule, the results are quite sensitive to the level of theory employed in the calculation. Compared to MP2, B3LYP clearly underestimates the electride character, whereas HF significantly overestimates it. CAM-B3LYP results agree quite well with the MP2 values, suggesting a rather small number of electrons in

Table 7. Results of the QTAIM Partitioning, EOS, and EDF Analyses for Li@calix[4]pyrrole[a]

method	basis	$\rho(\mathbf{r}_{NNA})$	$\nabla^2\rho(\mathbf{r}_{NNA})$	N_{NNA}	λ_{NNA}	EOS[1]	RI	EOS[2]	RI	P_0	P_1	P_2
CAM-B3LYP	ma-TZVP	7.6×10^{-3}	-4.0×10^{-3}	0.291	0.079	0	94	0	91	71.5	28.3	0.2
	aug-cc-pVTZ	8.0×10^{-3}	-5.2×10^{-3}	0.269	0.067	0	98	0	95	73.7	26.2	0.1
B3LYP	ma-TZVP	6.9×10^{-3}	-3.2×10^{-3}	0.215	0.043	0	100	0	100	78.9	21.0	0.1
	aug-cc-pVTZ	7.2×10^{-3}	-4.3×10^{-3}	0.193	0.035	0	100	0	100	81.0	18.9	0.1
M06-2X	ma-TZVP	7.0×10^{-3}	-2.9×10^{-3}	0.195	0.035	0	100	0	100	81.0	19.0	0.1
	aug-cc-pVTZ	7.3×10^{-3}	-4.1×10^{-3}	0.177	0.028	0	100	0	100	82.8	17.1	0.1
HF	ma-TZVP	7.6×10^{-3}	-5.2×10^{-3}	0.518	0.250	−0.5	100	−1	52	49.3	50.0	0.7
	aug-cc-pVTZ	7.8×10^{-3}	-5.8×10^{-3}	0.511	0.245	0	51	−1	51	49.8	49.5	0.6
MP2	ma-TZVP	7.7×10^{-3}	-4.5×10^{-3}	0.321	0.100					68.1	31.8	0.2
	aug-cc-pVTZ	8.2×10^{-3}	-5.6×10^{-3}	0.29	0.08					71.2	28.7	0.1

[a]For a full description, see Table 5.

Table 8. Results of the QTAIM partitioning, EOS, and EDF analyses for Na@calix[4]pyrrole[a]

method	basis	$\rho(\mathbf{r}_{NNA})$	$\nabla^2\rho(\mathbf{r}_{NNA})$	N_{NNA}	λ_{NNA}	EOS[1]	RI	EOS[2]	RI	P_0	P_1	P_2
CAM-B3LYP	ma-TZVP	5.9×10^{-3}	-2.6×10^{-3}	0.169	0.027	0	100	0	100	83.3	16.7	0.1
	aug-cc-pVTZ	6.0×10^{-3}	-2.6×10^{-3}	0.167	0.026	0	100	0	100	83.5	16.4	0.1
B3LYP	ma-TZVP	5.3×10^{-3}	-2.0×10^{-3}	0.094	0.008	0	100	0	100	90.8	9.2	0.0
	aug-cc-pVTZ	5.3×10^{-3}	-2.0×10^{-3}	0.086	0.007	0	100	0	100	91.5	8.5	0.0
M06-2X	ma-TZVP	5.7×10^{-3}	-2.2×10^{-3}	0.100	0.009	0	100	0	100	90.3	9.7	0.0
	aug-cc-pVTZ	5.5×10^{-3}	-1.8×10^{-3}	0.062	0.004	0	100	0	100	94.0	6.0	0.0
HF	ma-TZVP	5.8×10^{-3}	-3.1×10^{-3}	0.448	0.191	0	63	0	62	56.0	43.7	0.2
	aug-cc-pVTZ	6.0×10^{-3}	-3.4×10^{-3}	0.484	0.224	0	55	0	55	52.4	47.3	0.2
MP2	ma-TZVP	6.2×10^{-3}	-3.0×10^{-3}	0.202	0.041					79.8	20.2	0.0
	aug-cc-pVTZ	6.4×10^{-3}	-3.0×10^{-3}	0.195	0.039					80.5	19.6	0.0

[a]For a full description, see Table 5.

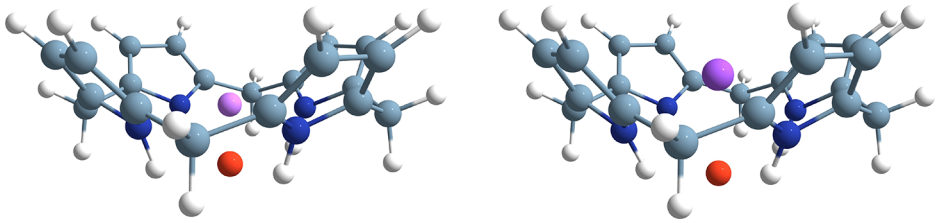

Figure 4. Geometries of Li@calix[4]pyrrole and Na@calix[4]pyrrole optimized at the CAM-B3LYP/ma-TZVP level of theory. The NNA position is indicated with a red ball.

Table 9. Results of the QTAIM Partitioning, EOS, and EDF Analyses for $TCNENa_3$[a]

method	basis	$\rho(\mathbf{r}_{NNA})$	$\nabla^2\rho(\mathbf{r}_{NNA})$	N_{NNA}	λ_{NNA}	EOS[1]	RI	EOS[2]	RI	P_0	P_1	P_2
CAM-B3LYP	ma-TZVP	7.0×10^{-3}	-4.4×10^{-3}	0.204	0.040	0	100	0	68	79.8	20.2	0.0
	aug-cc-pVTZ	7.2×10^{-3}	-4.9×10^{-3}	0.268	0.069	0	97	0	58	73.5	26.5	0.1
B3LYP	ma-TZVP	6.7×10^{-3}	-4.1×10^{-3}	0.162	0.025	0	100	0	74	84.0	16.0	0.0
	aug-cc-pVTZ	6.9×10^{-3}	-4.5×10^{-3}	0.218	0.046	0	100	0	66	78.5	21.5	0.0
M06-2X	ma-TZVP	6.8×10^{-3}	-4.0×10^{-3}	0.211	0.040	0	100	0	67	79.3	20.6	0.2
	aug-cc-pVTZ	7.1×10^{-3}	-4.6×10^{-3}	0.228	0.047	0	100	0	64	77.6	22.2	0.2
HF	ma-TZVP	7.1×10^{-3}	-5.2×10^{-3}	0.438	0.187	0	64	−1	66	56.6	43.3	0.1
	aug-cc-pVTZ	7.2×10^{-3}	-5.4×10^{-3}	0.495	0.238	0	52	−1	75	51.0	48.8	0.2
MP2	ma-TZVP	7.0×10^{-3}	-5.0×10^{-3}	0.410	0.165					59.1	40.7	0.2
	aug-cc-pVTZ	7.1×10^{-3}	-5.3×10^{-3}	0.464	0.211					53.8	46.0	0.2

[a]For a full description, see Table 5.

Table 10. Results of the QTAIM Partitioning, EOS, and EDF Analyses for $TCNENa_4$(II)[a]

method	basis	$\rho(\mathbf{r}_{NNA})$	$\nabla^2\rho(\mathbf{r}_{NNA})$	N_{NNA}	λ_{NNA}	EOS[1]	RI	EOS[2]	RI	P_0	P_1	P_2
CAM-B3LYP	ma-TZVP	7.0×10^{-3}	-4.3×10^{-3}	0.202	0.040	0	100	0	68	80.0	20.0	0.0
	aug-cc-pVTZ	7.2×10^{-3}	-4.9×10^{-3}	0.266	0.068	0	98	0	59	73.6	26.3	0.1
B3LYP	ma-TZVP	6.7×10^{-3}	-4.0×10^{-3}	0.159	0.024	0	100	0	74	84.3	15.7	0.0
	aug-cc-pVTZ	6.9×10^{-3}	-4.5×10^{-3}	0.215	0.045	0	100	0	66	78.7	21.2	0.0
M06-2X	ma-TZVP	6.8×10^{-3}	-4.0×10^{-3}	0.211	0.041	0	100	0	67	79.2	20.6	0.2
	aug-cc-pVTZ	7.1×10^{-3}	-4.6×10^{-3}	0.226	0.046	0	100	0	65	77.8	22.0	0.2
HF	ma-TZVP	7.1×10^{-3}	-5.2×10^{-3}	0.439	0.188	0	63	−1	67	56.5	43.4	0.1
	aug-cc-pVTZ	7.2×10^{-3}	-5.4×10^{-3}	0.495	0.239	0	52	−1	75	51.0	48.9	0.2
MP2	ma-TZVP	7.0×10^{-3}	-5.0×10^{-3}	0.411	0.166					59.1	40.8	0.2
	aug-cc-pVTZ	7.1×10^{-3}	-5.2×10^{-3}	0.465	0.211					53.8	46.0	0.2

[a]For the a full description, see Table 5.

the NNA basin. The EOS analysis clearly assigns a zero oxidation state, in line with the large value of the probability of finding no electron at the NNA (66−70%). However, there is a non-negligible probability of finding one electron (30−34%), suggesting that this is a low-electron-number molecular electride.

DISCUSSION AND CONCLUSIONS

In the previous section, we have seen that the correct description of a molecular electride hinges on the electronic structure method employed for the analyses. First of all, the basis set employed should include sufficiently flexible functions in the atoms that are close to the NNA; otherwise, the molecular electride character can be significantly under-

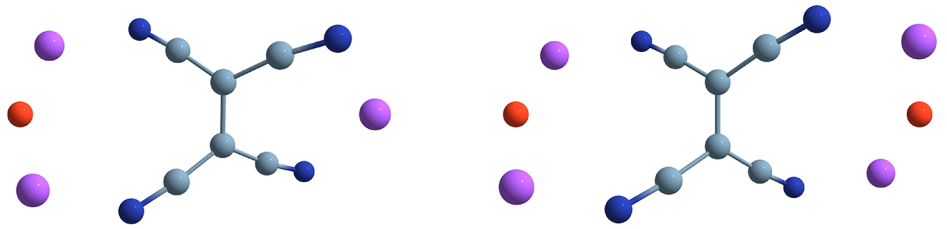

Figure 5. Geometries of $TCNENa_3$ and $TCNENa_4$(II) optimized at the CAM-B3LYP/ma-TZVP level of theory. The NNA position is indicated with a red ball.

Table 11. Results of the QTAIM Partitioning, EOS, and EDF Analyses for Mg_2EP[a]

method	basis	$\rho(\mathbf{r}_{NNA})$	$\nabla^2\rho(\mathbf{r}_{NNA})$	N_{NNA}	λ_{NNA}	EOS[1]	RI	EOS[2]	RI	P_0	P_1	P_2
CAM-B3LYP	ma-TZVP	3.2×10^{-2}	-3.8×10^{-2}	0.722	0.229	0	82	−2	59	42.1	44.7	12.8
	aug-cc-pVTZ	3.3×10^{-2}	-3.9×10^{-2}	0.746	0.244	0	80	−2	60	40.6	45.3	13.6
B3LYP	ma-TZVP	3.2×10^{-2}	-3.6×10^{-2}	0.677	0.201	0	87	−2	56	44.9	43.4	11.3
	aug-cc-pVTZ	3.2×10^{-2}	-3.8×10^{-2}	0.712	0.222	0	83	−2	58	42.7	44.4	12.4
M06-2X	ma-TZVP	3.1×10^{-2}	-3.6×10^{-2}	0.705	0.219	0	84	−2	58	43.1	44.3	12.2
	aug-cc-pVTZ	3.1×10^{-2}	-3.7×10^{-2}	0.701	0.216	0	84	−2	58	43.4	44.1	12.1
HF	ma-TZVP	3.4×10^{-2}	-4.3×10^{-2}	1.018	0.460	0	54	−2	79	25.8	48.8	24.3
	aug-cc-pVTZ	3.4×10^{-2}	-4.3×10^{-2}	1.030	0.470	0	53	−2	79	25.3	48.7	24.8
MP2	ma-TZVP	3.0×10^{-2}	-3.5×10^{-2}	0.835	0.332					34.8	46.9	18.3
	aug-cc-pVTZ	3.1×10^{-2}	-3.6×10^{-2}	0.876	0.366					32.5	47.4	20.1

[a]For a full description, see Table 5.

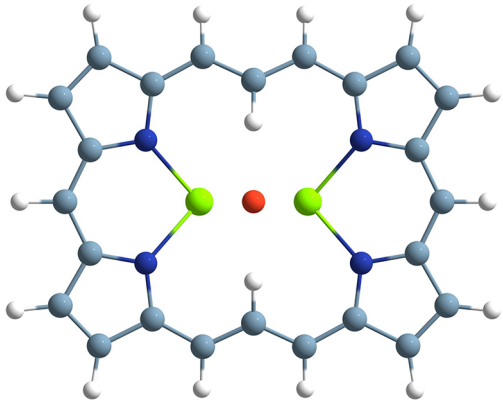

Figure 6. Geometry of Mg_2EP optimized at the CAM-B3LYP/ma-TZVP level of theory. The NNA position is indicated with a red ball.

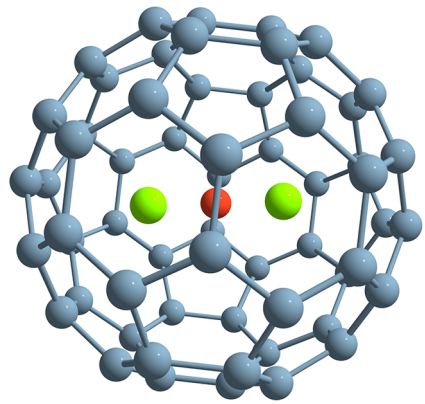

Figure 7. Geometry of $Mg_2@C_{60}$ optimized at the CAM-B3LYP/ma-TZVP level of theory. The NNA position is indicated with a red ball.

estimated, to the point that the molecule could not be considered an electride. This is the case of the ma-TZVP basis set, with which we cannot locate the NNA in some cases, whereas in other cases, we got a too small number of electrons in the NNA basins.

Among the density functional approximations explored in this work, CAM-B3LYP seems to be the one in closest agreement with the reference MP2 data. This is probably because range-separated functionals tend to reduce the delocalization error compared to their hybrid peers with a low percentage of HF exchange, such as B3LYP. In general, the

Table 12. Results of the QTAIM Partitioning, EOS, and EDF Analyses for $Mg_2@C_{60}$. For a full description, see Table 5

method	basis	$\rho(\mathbf{r}_{NNA})$	$\nabla^2\rho(\mathbf{r}_{NNA})$	N_{NNA}	λ_{NNA}	EOS[1]	RI	EOS[2]	RI	P_0	P_1	P_2
CAM-B3LYP	ma-TZVP	4.0×10^{-2}	-5.0×10^{-2}	0.699	0.211	0	85	−2	58	43.8	43.9	11.9
	aug-cc-pVTZ	4.0×10^{-2}	-5.5×10^{-2}	0.738	0.234	0	82	−2	61	41.4	44.9	13.1
B3LYP	ma-TZVP	3.9×10^{-2}	-5.0×10^{-2}	0.685	0.202	0	87	−2	57	44.8	43.4	11.4
	aug-cc-pVTZ	4.0×10^{-2}	-5.4×10^{-2}	0.732	0.229	0	82	−2	60	41.9	44.7	12.9
M06-2X	ma-TZVP	3.7×10^{-2}	-4.6×10^{-2}	0.687	0.203	0	86	−2	58	44.7	43.5	11.4
	aug-cc-pVTZ	3.8×10^{-2}	-5.2×10^{-2}	0.704	0.212	0	85	−2	59	43.7	43.9	12.0
HF	ma-TZVP	4.2×10^{-2}	-5.9×10^{-2}	0.971	0.404	0	60	−2	75	28.6	48.3	21.9
	aug-cc-pVTZ	4.2×10^{-2}	-6.2×10^{-2}	0.984	0.412	0	59	−2	76	28.0	48.3	22.3
MP2	ma-TZVP	3.3×10^{-2}	-3.7×10^{-2}	0.691	0.215					44.0	42.9	13.1

Table 13. Results of the QTAIM Partitioning, EOS, and EDF Analyses for $e@C_{60}F_{60}$[a]

method	basis	$\rho(\mathbf{r}_{NNA})$	$\nabla^2\rho(\mathbf{r}_{NNA})$	N_{NNA}	λ_{NNA}	EOS[1]	RI	P_0	P_1	P_2
CAM-B3LYP	6-31G+DF	3.99×10^{-3}	-3.77×10^{-3}	0.314	0.091	0	89	69.7	30.3	0.1
	6-31G(d)+DF	3.94×10^{-3}	-3.57×10^{-3}	0.318	0.093	0	88	69.4	30.6	0.0
	6-31+G+DF	2.85×10^{-3}	-9.90×10^{-4}	0.343	0.108	0	84	67.1	32.9	0.0
	ma-TZVP+DF	2.64×10^{-3}	-6.52×10^{-4}	0.354	0.114	0	83	66.0	33.8	0.2
B3LYP	6-31G+DF	3.26×10^{-3}	-3.07×10^{-3}	0.241	0.054	0	100	76.7	23.3	0.0
	6-31G(d)+DF	3.24×10^{-3}	-2.92×10^{-3}	0.247	0.057	0	100	76.1	23.8	0.0
	6-31+G+DF	2.35×10^{-3}	-8.38×10^{-4}	0.253	0.059	0	100	75.6	24.4	0.0
	ma-TZVP+DF	2.18×10^{-3}	-5.76×10^{-4}	0.268	0.065	0	99	74.4	25.6	0.0
HF	6-31G+DF	6.73×10^{-3}	-7.52×10^{-3}	0.506	0.236	0	52	51.2	48.6	0.2
	6-31G(d)+DF	6.55×10^{-3}	-7.12×10^{-3}	0.504	0.234	0	53	51.6	48.4	0.1
	6-31+G+DF	4.70×10^{-3}	-2.54×10^{-3}	0.569	0.296	−1	59	45.2	54.4	0.5
	ma-TZVP+DF	4.35×10^{-3}	-1.70×10^{-3}	0.594	0.319	−1	59	43.2	56.3	0.5
	cc-pVDZ+DF	6.24×10^{-3}	-6.58×10^{-3}	0.483	0.213	0	57	53.8	46.2	0.1
MP2	6-31G+DF	4.05×10^{-3}	-3.40×10^{-3}	0.337	0.111			68.6	31.4	0.0
	6-31G(d)+DF	3.57×10^{-3}	-2.61×10^{-3}	0.314	0.098			64.5	35.2	0.2
	6-31+G+DF	2.51×10^{-3}	-7.78×10^{-5}	0.357	0.123			66.4	33.4	0.2

[a]For a full description, see Table 5.

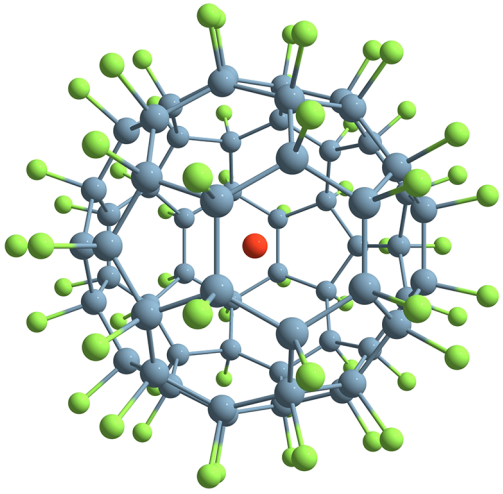

Figure 8. Geometry of $e@C_{60}F_{60}$ optimized at the CAM-B3LYP/ma-TZVP+DF level of theory. The NNA position is indicated with a red ball.

number of electrons in the NNA basins of electrides depends on the amount of HF exchange included in the method. B3LYP usually gives the lowest average electron numbers in the NNA basins, the largest zero-electron probabilities, and the lowest oxidation states. This result is in line with the large delocalization errors documented in conjugated[82] and aromatic molecules.[83−86,95] CAM-B3LYP and M06-2X do not suffer from large delocalization errors and often provide similar NNA electron numbers, although slightly lower than those given by MP2. On the other hand, HF, which tends to overestimate electron localization, provides the largest electron numbers in the NNA basin. This is the general trend but, in other cases, such as Mg_2EP, the delocalization error does not seem to be so important and all density functional approximations underestimate the electride character. One should keep in mind that some DFAs are completely inadequate to study molecular electrides. This is the case of MN15,[99] which systematically fails to locate an NNA in these molecules. For the sake of completeness, we have included these results in the Supporting Information.

Several tools to analyze the electride character of molecules have been employed in this work. If we take as a reference criterion the probability of finding at least one electron in the NNA basin, $1 - P_0$, we realize that there is not a clear-cut value of the electron density at the NNA or its Laplacian that can be used to clearly characterize the molecule (see Figures S2 and S3). The same can be said about the average number of electrons in the NNA and the localization index. However, as a qualitative indication, we can state that one-electron electrides ($1 - P_0 > 0.5$) usually have $N_{NNA} \geq 0.5$ and $\lambda_{NNA} \geq 0.2$ (see Figures S4 and S5). In most cases, the EOS analysis predicts an oxidation state in agreement with the largest probability. However, we have found some exceptions to analyze in detail: $Mg_2@C_{60}$ and Mg_2EP.

First of all, we will examine the EOS analysis that applies the simplest fragmentation, EOS[1], which only considers two fragments: the NNA and the rest of the molecule. Instead of the reliability index (RI), which only takes values in the range [50%, 100%], we will analyze the smallest difference between the occupation of the lowest occupied effective atomic orbital (EffAO), λ_{LO}, and the first unoccupied orbital, λ_{FU}, i.e., $\min(\Delta\lambda^{\alpha},\Delta\lambda^{\beta})$. Notice that by *occupied* and *unoccupied* EffAOs, we refer to orbitals to which at least one electron is and is not assigned, respectively, during the EOS analysis. $\Delta\lambda = \lambda_{LO} - \lambda_{FU}$ is actually used to calculate the RI (see eq 11) and, in practice, employing this measure instead of the RI will permit to distinguish cases that will be all considered 100% certain by the RI (compare Figures 9 and S1). Furthermore, $\Delta\lambda = 0$ does not imply that the probability of the oxidation states assigned by the EOS analysis is 50% since $\Delta\lambda = 0$ can also occur when we have systems with more than two oxidation states that have the same probability. In Figure 9, we represent the probability of finding n electrons at the NNA basin, n being the oxidation state predicted by the EOS analysis, against $\min(\Delta\lambda^{\alpha},\Delta\lambda^{\beta})$ for all the molecules and methods for which we could locate an NNA. We can clearly differentiate between two groups of molecules: types A and B. Each group shows a perfectly predictable behavior of one quantity with respect to the other. Type-B electrides correspond to calculations for which P_2 is negligible, whereas P_2 values are significant ($P_2 > 0.1$) for type-A electrides. For type-B electrides, which are open-shell molecules, there is only one EffAO assigned to the NNA with

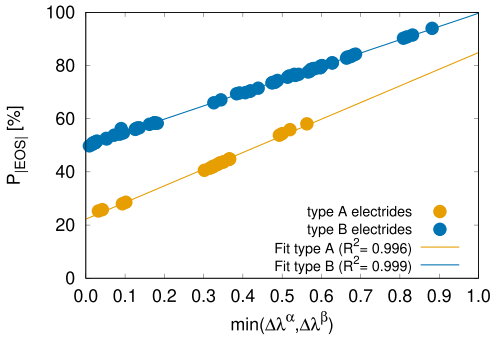

Figure 9. Probability of finding in the NNA basin the number of electrons predicted by the EOS analysis ($P_{|EOS|}$) against min-($\Delta\lambda^{\alpha}$,$\Delta\lambda^{\beta}$). $\Delta\lambda$ and EOS analysis were obtained with the type 1 fragmentation. The plot includes data for all methods and basis sets (excluding MP2) for which one NNA was found.

an occupation much larger than zero, λ, which, has a corresponding EffAOs in the other fragment with occupation $1 - \lambda$ (the other occupied and unoccupied EffAOs assigned to the rest of the molecule have occupations close to 1 and 0, respectively). For single-determinant wave functions, if $P_i = 0$ $\forall i > 1$, $P_0 = (1 - \lambda)$ and $P_1 = \lambda$, it is easy to prove that $P_i = {}^1/_2 + {}^1/_2\Delta\lambda$, i being the oxidation state assigned by the EOS analysis (in this case, i is either zero or one) and the gap being $\Delta\lambda = |1 - 2\lambda|$. Indeed, the blue points in Figure 9 follow this equation. Type-A electrides are closed-shell molecules, for which P_2 is not negligible, $P_i = 0$ $\forall i > 2$ and, by spin symmetry, they have only two degenerate EffAOS with occupations $\lambda_1 = \lambda_2 = \lambda$. In this case, the probabilities can also be determined analytically for the oxidation state assigned by EOS. By spin symmetry, the EOS analysis can only assign zero or two electrons to the NNA of type-A electrides and, in either case, $P = {}^1/_4(\Delta\lambda + 1)^2$, so there is also a simple relationship between the gap and the probability, but this time there is a quadratic dependence. For $\Delta\lambda < {}^1/_2$, the error of neglecting the quadratic term in calculating P leads to small errors, ranging between 0% and 6.25%. For this reason, type-A electrides, which mostly have $\Delta\lambda$ values below ${}^1/_2$, also present an excellent linear correlation between P with $\Delta\lambda$ (see Figure 9).

From the latter results, some features of the EOS analysis are revealed. Since α and β electrons are assigned independently, symmetry-breaking electron distributions of the fragments are not considered in the EOS analysis—this fact is reminiscent of the incompatibility[140] of the local spin analysis[141,142] and the EDFs. This is a consequence of EOS (or local spin) considering averaged quantities, whereas EDFs are probabilities that can include symmetry-breaking situations (obviously, EDFs can be used to calculate averaged quantities that will respect the symmetry of the system, see eq 3). Hence, the EOS analysis on the fragment partitions of closed-shell molecules will never assign an odd number of electrons to some fragment, and therefore, there will never be an agreement between the EOS and EDFs analyses for the fragments of closed-shell molecules for which the largest P_i corresponds to an odd i.

In the following, we will discuss some advantages of using $\Delta\lambda^{\alpha}\Delta\lambda^{\beta}$ instead of RI to measure the reliability of the oxidation state provided by the EOS analysis. As stated above, the RI depends on min($\Delta\lambda^{\alpha}$,$\Delta\lambda^{\beta}$) value (see eq 10). We have found a linear correspondence between min($\Delta\lambda^{\alpha}$,$\Delta\lambda^{\beta}$) and the EDFs for some simple systems, such as type-B electrides, for which $P_i \approx 0$ $\forall i > 1$ and, therefore, $\Delta\lambda^{\beta} \approx 1$. However, for the type-A electrides, the quadratic dependence of P on $\Delta\lambda^{\alpha}\Delta\lambda^{\beta}$ is not negligible, and the relationship between the RI and the probability is lost in this case. For this reason, we believe that $\Delta\lambda^{\alpha}\Delta\lambda^{\beta}$ is a better measure of the uncertainty of the oxidation state assignment. In Figure 10, we display the probability of having a number of electrons that matches the oxidation state predicted by the EOS analysis for type-A and type-B electrides against this new measure of uncertainty. For type-B molecules, as discussed above, the dependence of P on $\Delta\lambda^{\alpha}\Delta\lambda^{\beta}$ is very similar to the one presented in Figure 9 because $\Delta\lambda^{\beta} \approx 1$. In this figure, for type-A electrides, we also represent the probability of having zero, one, and two electrons in the NNA basins. For the type-A electrides, the EOS analysis always predicts a zero oxidation state. However, for several of these molecules, P_1 is larger than P_0 and the values of $\Delta\lambda^{\alpha}\Delta\lambda^{\beta}$ are really small. In fact, the latter quantity is smaller than 0.3 until the probability of having no electrons goes well beyond 50%. In this sense, this new reliability measure seems to display small values for systems with more distributed probabilities, such as those in the type-A category, and only provides very large values (close to 1.0) for cases where the probability of having exactly the number of electrons indicated by the oxidation state is close to 100%. Notice that the oxidation state assignment provided by the EOS analysis remains unchanged; we are only suggesting a reliability measure that better reflects the probabilities given by the EDFs,

$$\mathrm{RM} = \Delta\lambda^{\alpha}\Delta\lambda^{\beta} \tag{12}$$

with RM taking values between zero and one. As an illustration, let us compare RI and RM values for $Mg_2@C_{60}$ at the CAM-B3LYP/ma-TZVP level of theory. In this case, EOS[1] = 0 with RI = 85% (a highly reliable assignment), and EOS[2] = −2 with RI = 58%. On the other hand, RM is equal to 0.12, a fairly small value for EOS[1], in better agreement with the EDFs, which state that P_1 value is very close to P_0 and $1 - P_0 > 0.5$.

The second partition considered in the EOS analysis, which defines separate fragments for the metallic atoms in the molecules (Li, Na, and Mg), always provides an oxidation state equal or more negative than the first partition. If the NNA and the rest of the molecule are competing for an electron, it is more likely for the NNA to win the battle when the rest of the molecule is divided into various fragments. If we disregard the

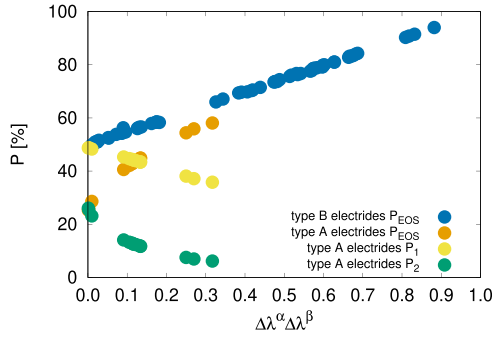

Figure 10. Probability of finding of finding 0, 1, or 2 electrons in the NNA basin against RM (see eq 11). $\Delta\lambda$ and EOS analysis were obtained with the type 1 fragmentation. The plot includes data for all methods and basis sets (excluding MP2) for which one NNA was found.

situations where the quality of the basis set was dubious and HF (which clearly overestimates the localized character of the NNA), most of the discrepancies between EOS[1] and EOS[2] occurred for type-A electrides. In other words, the partition seems to be more relevant in situations where $P_2 \gg 0$ and the RM value is small.

We have studied nine molecular electrides in this paper. Three of them are classified as one-electron electrides ($1 - P_0 > 0.5$): $TCNQLi_2$, Mg_2EP, and $Mg_2@C_{60}$. Other three show an intermediate situation between zero- and one-electron electrides ($P_0 \approx 0.5$), $TCNQNa_2$, $TCNENa_3$, and $TCNENa_4$(II). Finally, the other three molecular electrides are classified as low-electron-number electrides ($0.5 \gg 1 - P_0 \gg 0$), Li@calix[4]pyrrole, Na@calix[4]pyrrole, and $e@C_{60}F_{60}$. We believe this classification highlights *the strength of the electride character* and will prove useful in the design of new electrides.

■ ASSOCIATED CONTENT

Supporting Information

The Supporting Information is available free of charge at https://pubs.acs.org/doi/10.1021/acs.jpca.1c02760.

Calculated static NLOPs of $TCNENa_3$ and $TCNENa_4$(II), results obtained with the MN15 density functional approximation, and correlation plots between various descriptors of the NNA character (PDF)

Cartesian coordinates of all the molecules (optimized at the CAM-B3LYP/ma-TZVP level of theory) (XYZ)

■ AUTHOR INFORMATION

Corresponding Authors

Eloy Ramos-Cordoba − *Donostia International Physics Center (DIPC), 20018 Donostia, Euskadi, Spain; Polimero eta Material Aurreratuak: Fisika, Kimika eta Teknologia, Kimika Fakultatea, Euskal Herriko Unibertsitatea UPV/EHU, 20080 Donostia, Euskadi, Spain;* orcid.org/0000-0002-6558-7821; Email: eloy.raco@gmail.com

Josep M. Luis − *Institut de Química Computacional i Catàlisi (IQCC) and Departament de Química, Universitat de Girona, 17003 Girona, Catalonia, Spain;* orcid.org/0000-0002-2880-8680; Email: josepm.luis@udg.edu

Eduard Matito − *Donostia International Physics Center (DIPC), 20018 Donostia, Euskadi, Spain; Ikerbasque Foundation for Science, 48009 Bilbao, Euskadi, Spain;* orcid.org/0000-0001-6895-4562; Email: ematito@gmail.com

Author

Sebastian P. Sitkiewicz − *Donostia International Physics Center (DIPC), 20018 Donostia, Euskadi, Spain; Polimero eta Material Aurreratuak: Fisika, Kimika eta Teknologia, Kimika Fakultatea, Euskal Herriko Unibertsitatea UPV/EHU, 20080 Donostia, Euskadi, Spain*

■ ACKNOWLEDGMENTS

The authors are indebted to Dr. Pedro Salvador for helpful discussions and an anonymous reviewer for an insightful observation about MP2 probabilities. This work has been supported by grants from the Spanish government MICINN (PGC2018-098212−B-C21, PGC2018-098212−B-C22, CTQ2016-80375-P, and EUR2019-103825), Generalitat de Catalunya (2017SGR39), Diputación Foral de Gipuzkoa (2019-CIEN-000092-01). and Gobierno Vasco-Eusko Jaurlaritza (IT1254-19, PRE_2020_2_0015 and PIBA19-0004). E.R.-C. acknowledges funding from the Juan de la Cierva Program IJCI-2017-34658. We are also grateful for the computational time from the Consorci de Serveis Universitaris de Catalunya (CSUC), DIPC, and the SGI/IZO-SGIker UPV/EHU.

■ REFERENCES

(1) Dye, J. L. Electrons as anions. *Science* **2003**, *301*, 607−608.

(2) Dye, J. L. Electrides: ionic salts with electrons as the anions. *Science* **1990**, *247*, 663−668.

(3) Dye, J. L.; DeBacker, M. G. Physical and chemical properties of alkalides and electrides. *Annu. Rev. Phys. Chem.* **1987**, *38*, 271−299.

(4) Dye, J. L. Electrides: early examples of quantum confinement. *Acc. Chem. Res.* **2009**, *42*, 1564−1572.

(5) Dye, J. L.; Ceraso, J. M.; Lok, M.; Barnett, B.; Tehan, F. J. Crystalline salt of the sodium anion (Na^-). *J. Am. Chem. Soc.* **1974**, *96*, 608−609.

(6) Ellaboudy, A.; Dye, J. L.; Smith, P. B. Cesium 18-crown-6 compounds. A crystalline ceside and a crystalline electride. *J. Am. Chem. Soc.* **1983**, *105*, 6490−6491.

(7) Dawes, S. B.; Ward, D. L.; Huang, R. H.; Dye, J. L. First electride crystal structure. *J. Am. Chem. Soc.* **1986**, *108*, 3534−3535.

(8) Dye, J. L. Anionic electrons in electrides. *Nature* **1993**, *365*, 10−11.

(9) Dye, J. L. Electrides: From 1D Heisenberg chains to 2D pseudo-metals. *Inorg. Chem.* **1997**, *36*, 3816−3826.

(10) Redko, M. Y.; Jackson, J. E.; Huang, R. H.; Dye, J. L. Design and synthesis of a thermally stable organic electride. *J. Am. Chem. Soc.* **2005**, *127*, 12416−12422.

(11) Matsuishi, S.; Toda, Y.; Miyakawa, M.; Hayashi, K.; Kamiya, T.; Hirano, M.; Tanaka, I.; Hosono, H. High-density electron anions in a nanoporous single crystal: $[Ca_{24}Al_{28}O_{64}]^{4+}(4e^-)$. *Science* **2003**, *301*, 626−629.

(12) Toda, Y.; Yanagi, H.; Ikenaga, E.; Kim, J. J.; Kobata, M.; Ueda, S.; Kamiya, T.; Hirano, M.; Kobayashi, K.; Hosono, H. Work function of a room-temperature, stable electride $[Ca_{24}Al_{28}O_{64}]^{4+}(4e^-)$. *Adv. Mater.* **2007**, *19*, 3564−3569.

(13) Yanagi, H.; Kuroda, T.; Kim, K.-B.; Toda, Y.; Kamiya, T.; Hosono, H. Electron injection barriers between air-stable electride with low work function, $C_{12}A_7{:}e^-$, and pentacene, C_{60} and copper phthalocyanine. *J. Mater. Chem.* **2012**, *22*, 4278−4281.

(14) Buchammagari, H.; Toda, Y.; Hirano, M.; Hosono, H.; Takeuchi, D.; Osakada, K. Room temperature-stable electride as a synthetic organic reagent: application to pinacol coupling reaction in aqueous media. *Org. Lett.* **2007**, *9*, 4287−4289.

(15) Yanagi, H.; Kim, K.-B.; Koizumi, I.; Kikuchi, M.; Hiramatsu, H.; Miyakawa, M.; Kamiya, T.; Hirano, M.; Hosono, H. Low threshold voltage and carrier injection properties of inverted organic light-emitting diodes with $[Ca_{24}Al_{28}O_{64}]^{4+}(4e^-)$ cathode and $Cu_{2-x}Se$ anode. *J. Phys. Chem. C* **2009**, *113*, 18379−18384.

(16) Hayashi, K. Heavy doping of H^- ion in $12CaO{\cdot}7Al_2O_3$. *J. Solid State Chem.* **2011**, *184*, 1428−1432.

(17) Kitano, M.; Inoue, Y.; Yamazaki, Y.; Hayashi, F.; Kanbara, S.; Matsuishi, S.; Yokoyama, T.; Kim, S.-W.; Hara, M.; Hosono, H. Ammonia synthesis using a stable electride as an electron donor and reversible hydrogen store. *Nat. Chem.* **2012**, *4*, 934−940.

(18) Li, J.; Yin, B.; Fuchigami, T.; Inagi, S.; Hosono, H.; Ito, S. Application of $12CaO \cdot 7Al_2O_3$ electride as a new electrode for superoxide ion generation and hydroxylation of an arylboronic acid. *Electrochem. Commun.* **2012**, *17*, 52−55.

(19) Kamiya, T.; Aiba, S.; Miyakawa, M.; Nomura, K.; Matsuishi, S.; Hayashi, K.; Ueda, K.; Hirano, M.; Hosono, H. Field-Induced Current

Modulation in Nanoporous Semiconductor, Electron-Doped 12CaO · $7Al_2O_3$. *Chem. Mater.* **2005**, *17*, 6311−6316.
(20) Watanabe, S.; Watanabe, T.; Ito, K.; Miyakawa, N.; Ito, S.; Hosono, H.; Mikoshiba, S. Secondary electron emission and glow discharge properties of 12CaO· $7Al_2O_3$ electride for fluorescent lamp applications. *Sci. Technol. Adv. Mater.* **2011**, *12*, 034410.
(21) Kim, S. W.; Shimoyama, T.; Hosono, H. Solvated electrons in high-temperature melts and glasses of the room-temperature stable electride $[Ca_{24}Al_{28}O_{64}]^{4+}\cdot 4e-$. *Science* **2011**, *333*, 71−74.
(22) Mizoguchi, H.; Okunaka, M.; Kitano, M.; Matsuishi, S.; Yokoyama, T.; Hosono, H. Hydride-based electride material, LnH_2 (Ln = La, Ce, or Y). *Inorg. Chem.* **2016**, *55*, 8833−8838.
(23) Chanhom, P.; Fritz, K. E.; Burton, L. A.; Kloppenburg, J.; Filinchuk, Y.; Senyshyn, A.; Wang, M.; Feng, Z.; Insin, N.; Suntivich, J.; et al. Sr_3CrN_3: A new electride with a partially filled d-shell transition metal. *J. Am. Chem. Soc.* **2019**, *141*, 10595−10598.
(24) Zhang, Y.; Wang, B.; Xiao, Z.; Lu, Y.; Kamiya, T.; Uwatoko, Y.; Kageyama, H.; Hosono, H. Electride and superconductivity behaviors in Mn_5Si_3-type intermetallics. *Npj Quantum Mater.* **2017**, *2*, 45.
(25) Wang, J.; Hanzawa, K.; Hiramatsu, H.; Kim, J.; Umezawa, N.; Iwanaka, K.; Tada, T.; Hosono, H. Exploration of stable strontium phosphide-based electrides: Theoretical structure prediction and experimental validation. *J. Am. Chem. Soc.* **2017**, *139*, 15668−15680.
(26) Zhang, Y.; Xiao, Z.; Kamiya, T.; Hosono, H. Electron confinement in channel spaces for one-dimensional electride. *J. Phys. Chem. Lett.* **2015**, *6*, 4966−4971.
(27) Lee, K.; Kim, S. W.; Toda, Y.; Matsuishi, S.; Hosono, H. Dicalcium nitride as a two-dimensional electride with an anionic electron layer. *Nature* **2013**, *494*, 336−340.
(28) Lee, S. Y.; Hwang, J.-Y.; Park, J.; Nandadasa, C. N.; Kim, Y.; Bang, J.; Lee, K.; Lee, K. H.; Zhang, Y.; Ma, Y.; et al. Ferromagnetic quasi-atomic electrons in two-dimensional electride. *Nat. Commun.* **2020**, *11*, 1526.
(29) Lu, Y.; Wang, J.; Li, J.; Wu, J.; Kanno, S.; Tada, T.; Hosono, H. Realization of Mott-insulating electrides in dimorphic Yb_5Sb_3. *Phys. Rev. B: Condens. Matter Mater. Phys.* **2018**, *98*, 125128.
(30) Lu, Y.; Tada, T.; Toda, Y.; Ueda, S.; Wu, J.; Li, J.; Horiba, K.; Kumigashira, H.; Zhang, Y.; Hosono, H. Interlayer states arising from anionic electrons in the honeycomb-lattice-based compounds *Ae*AlSi (*Ae* = Ca, Sr, Ba). *Phys. Rev. B: Condens. Matter Mater. Phys.* **2017**, *95*, 125117.
(31) Yan, J.-Q.; Ochi, M.; Cao, H. B.; Saparov, B.; Cheng, J.-G.; Uwatoko, Y.; Arita, R.; Sales, B. C.; Mandrus, D. G. Magnetic order of Nd_5Pb_3 single crystals. *J. Phys.: Condens. Matter* **2018**, *30*, 135801.
(32) Kang, S. H.; Bang, J.; Chung, K.; Nandadasa, C. N.; Han, G.; Lee, S.; Lee, K. H.; Lee, K.; Ma, Y.; Oh, S. H.; et al. Water- and acid-stable self-passivated dihafnium sulfide electride and its persistent electrocatalytic reaction. *Sci. Adv.* **2020**, *6*, No. eaba7416.
(33) Druffel, D. L.; Kuntz, K. L.; Woomer, A. H.; Alcorn, F. M.; Hu, J.; Donley, C. L.; Warren, S. C. Experimental Demonstration of an Electride as a 2D Material. *J. Am. Chem. Soc.* **2016**, *138*, 16089−16094.
(34) Druffel, D. L.; Woomer, A. H.; Kuntz, K. L.; Pawlik, J. T.; Warren, S. C. Electrons on the surface of 2D materials: from layered electrides to 2D electrenes. *J. Mater. Chem. C* **2017**, *5*, 11196−11213.
(35) Wu, J.; Gong, Y.; Inoshita, T.; Fredrickson, D. C.; Wang, J.; Lu, Y.; Kitano, M.; Hosono, H. Tiered electron anions in multiple voids of LaScSi and their applications to ammonia synthesis. *Adv. Mater.* **2017**, *29*, 1700924.
(36) Ye, T.-N.; Lu, Y.; Li, J.; Nakao, T.; Yang, H.; Tada, T.; Kitano, M.; Hosono, H. Copper-based intermetallic electride catalyst for chemoselective hydrogenation reactions. *J. Am. Chem. Soc.* **2017**, *139*, 17089−17097.
(37) Wu, J.; Li, J.; Gong, Y.; Kitano, M.; Inoshita, T.; Hosono, H. Intermetallic electride catalyst as a platform for ammonia synthesis. *Angew. Chem., Int. Ed.* **2019**, *58*, 825−829.
(38) Li, J.; Wu, J.; Wang, H.; Lu, Y.; Ye, T.; Sasase, M.; Wu, X.; Kitano, M.; Inoshita, T.; Hosono, H. Acid-durable electride with layered ruthenium for ammonia synthesis: boosting the activity via selective etching. *Chem. Sci.* **2019**, *10*, 5712−5718.
(39) Mizoguchi, H.; Park, S.-W.; Kishida, K.; Kitano, M.; Kim, J.; Sasase, M.; Honda, T.; Ikeda, K.; Otomo, T.; Hosono, H. Zeolitic Intermetallics: LnNiSi (Ln = La−Nd). *J. Am. Chem. Soc.* **2019**, *141*, 3376−3379.
(40) Ye, T.-N.; Lu, Y.; Xiao, Z.; Li, J.; Nakao, T.; Abe, H.; Niwa, Y.; Kitano, M.; Tada, T.; Hosono, H. Palladium-bearing intermetallic electride as an efficient and stable catalyst for Suzuki cross-coupling reactions. *Nat. Commun.* **2019**, *10*, 5653.
(41) Hu, Q.; Tan, R.; Yao, W.; Cui, Y.; Li, J.; Song, W. Preparation and X-ray photoelectron spectroscopic characterization of Sn-doped $C_{12}A_7$:e^- electride nanoparticles. *Appl. Surf. Sci.* **2020**, *508*, 145244.
(42) Lu, Y.; Li, J.; Ye, T.-N.; Kobayashi, Y.; Sasase, M.; Kitano, M.; Hosono, H. Synthesis of rare-earth-based metallic electride nanoparticles and their catalytic applications to selective hydrogenation and ammonia synthesis. *ACS Catal.* **2018**, *8*, 11054−11058.
(43) He, H.-M.; Li, Y.; Yang, H.; Yu, D.; Li, S.-Y.; Wu, D.; Hou, J.-H.; Zhong, R.-L.; Zhou, Z.-J.; Gu, F.-L.; et al. Efficient external electric field manipulated nonlinear optical switches of all-metal electride molecules with infrared transparency: nonbonding electron transfer forms an excess electron lone pair. *J. Phys. Chem. C* **2017**, *121*, 958−968.
(44) He, H.-M.; Luis, J. M.; Chen, W.-H.; Yu, D.; Li, Y.; Wu, D.; Sun, W.-M.; Li, Z.-R. Nonlinear optical response of endohedral all-metal electride cages $2e^-$ $Mg^{2+}(M@E_{12})^{2-}$ Ca^{2+}(M= Ni, Pd, and Pt; E= Ge, Sn, and Pb). *J. Mater. Chem. C* **2019**, *7*, 645−653.
(45) Postils, V.; Garcia-Borrás, M.; Solà, M.; Luis, J. M.; Matito, E. On the existence and characterization of molecular electrides. *Chem. Commun.* **2015**, *51*, 4865−4868.
(46) El Bakouri, O.; Postils, V.; Garcia-Borràs, M.; Duran, M.; Luis, J. M.; Calvello, S.; Soncini, A.; Matito, E.; Feixas, F.; Solà, M. Metal cluster electrides: A new type of molecular electride with delocalised polyattractor character. *Chem. - Eur. J.* **2018**, *24*, 9853−9859.
(47) Marqués, M.; Ackland, G. J.; Lundegaard, L. F.; Stinton, G.; Nelmes, R. J.; McMahon, M. I.; Contreras-García, J. Potassium under pressure: A pseudobinary ionic compound. *Phys. Rev. Lett.* **2009**, *103*, 115501.
(48) Marqués, M.; McMahon, M.; Gregoryanz, E.; Hanfland, M.; Guillaume, C.; Pickard, C.; Ackland, G.; Nelmes, R. Crystal structures of dense lithium: a metal-semiconductor-metal transition. *Phys. Rev. Lett.* **2011**, *106*, 095502.
(49) Gatti, M.; Tokatly, I. V.; Rubio, A. Sodium: a charge-transfer insulator at high pressures. *Phys. Rev. Lett.* **2010**, *104*, 216404.
(50) Li, P.; Gao, G.; Wang, Y.; Ma, Y. Crystal structures and exotic behavior of magnesium under pressure. *J. Phys. Chem. C* **2010**, *114*, 21745−21749.
(51) Becke, A. D.; Edgecombe, K. E. A simple mesure of electron localization in atomic and molecular systems. *J. Chem. Phys.* **1990**, *92*, 5397−5403.
(52) Miao, M.-S.; Hoffmann, R. High pressure electrides: The chemical nature of interstitial quasiatoms. *J. Am. Chem. Soc.* **2015**, *137*, 3631−3637.
(53) Miao, M.-S.; Hoffmann, R. High pressure electrides: A predictive chemical and physical theory. *Acc. Chem. Res.* **2014**, *47*, 1311−1317.
(54) Ward, D. L.; Huang, R. H.; Dye, J. L. Structures of alkalides and electrides. I. Structure of potassium cryptand[2.2.2] electride. *Acta Crystallogr., Sect. C: Cryst. Struct. Commun.* **1988**, *44*, 1374−1376.
(55) Huang, R. H.; Faber, M. K.; Moeggenborg, K. J.; Ward, D. L.; Dye, J. L. Structure of K^+(cryptand[2.2.2]) electride and evidence for trapped electron pairs. *Nature* **1988**, *331*, 599−601.
(56) Dawes, S. B.; Eglin, J. L.; Moeggenborg, K. J.; Kim, J.; Dye, J. L. Cs^+(15-crown-5)$_2\cdot e^-$. A crystalline antiferromagnetic electride. *J. Am. Chem. Soc.* **1991**, *113*, 1605−1609.
(57) Wagner, M. J.; Huang, R. H.; Eglin, J. L.; Dye, J. L. An electride with a large six-electron ring. *Nature* **1994**, *368*, 726−729.
(58) Huang, R. H.; Wagner, M. J.; Gilbert, D. J.; Reidy-Cedergren, K. A.; Ward, D. L.; Faber, M. K.; Dye, J. L. Structure and properties of

Li^+(cryptand [2.1.1])e^-, an electride with a 1D "spin-ladder-like" cavity-channel geometry. *J. Am. Chem. Soc.* **1997**, *119*, 3765−3772.
(59) Xie, Q.; Huang, R. H.; Ichimura, A. S.; Phillips, R. C.; Pratt, W. P.; Dye, J. L. Structure and properties of a new electride, Rb^+(cryptand[2.2.2])e^-. *J. Am. Chem. Soc.* **2000**, *122*, 6971−6978.
(60) Zhang, X.; Xiao, Z.; Lei, H.; Toda, Y.; Matsuishi, S.; Kamiya, T.; Ueda, S.; Hosono, H. Two-dimensional transition-metal electride Y_2C. *Chem. Mater.* **2014**, *26*, 6638−6643.
(61) Lu, Y.; Li, J.; Tada, T.; Toda, Y.; Ueda, S.; Yokoyama, T.; Kitano, M.; Hosono, H. Water durable electride Y_5Si_3: Electronic structure and catalytic activity for ammonia synthesis. *J. Am. Chem. Soc.* **2016**, *138*, 3970−3973.
(62) Hara, M.; Kitano, M.; Hosono, H. Ru-loaded $C_{12}A_7$:e^- electride as a catalyst for ammonia synthesis. *ACS Catal.* **2017**, *7*, 2313−2324.
(63) Faseela, K. P.; Kim, Y. J.; Kim, S.-G.; Kim, S. W.; Baik, S. Dramatically enhanced stability of silver passivated dicalcium nitride electride: Ag-Ca_2N. *Chem. Mater.* **2018**, *30*, 7803−7812.
(64) Xiao, Y.; Zhang, X.; Li, R.; Zhang, J. Rapid synthesis and electric transport properties of $(Ca_{1-x}Ba_x)12Al_{14}O_{33}$ electrides. *J. Electron. Mater.* **2020**, *49*, 2471−2478.
(65) Zhang, X.; Feng, Q.; Zhao, J.; Liu, H.; Li, J.; Xiao, Y.; Li, F.; Lu, Q. Sr-doping enhanced electrical transport and thermionic emission of single crystal $12CaO \cdot 7Al_2O_3$ electride. *Curr. Appl. Phys.* **2020**, *20*, 96−101.
(66) Dale, S. G.; Johnson, E. R. Theoretical descriptors of electrides. *J. Phys. Chem. A* **2018**, *122*, 9371−9391.
(67) Miyakawa, M.; Kim, S. W.; Hirano, M.; Kohama, Y.; Kawaji, H.; Atake, T.; Ikegami, H.; Kono, K.; Hosono, H. Superconductivity in an inorganic electride $12CaO \cdot 7Al_2O_3$:e^-. *J. Am. Chem. Soc.* **2007**, *129*, 7270−7271.
(68) He, Y. The structural, electronic, elastic and thermodynamics properties of 2D transition-metal electride Y2C via first-principles calculations. *J. Alloys Compd.* **2016**, *654*, 180−184.
(69) Ge, Y.; Guan, S.; Liu, Y. Two dimensional superconductors in electrides. *New J. Phys.* **2017**, *19*, 123020.
(70) Chen, W.; Li, Z.-R.; Wu, D.; Li, Y.; Sun, C.-C.; Gu, F. L. The structure and the large nonlinear optical properties of Li@calix[4] pyrrole. *J. Am. Chem. Soc.* **2005**, *127*, 10977−10981.
(71) Garcia-Borràs, M.; Solà, M.; Luis, J. M.; Kirtman, B. Electronic and vibrational nonlinear optical properties of five representative electrides. *J. Chem. Theory Comput.* **2012**, *8*, 2688−2697.
(72) Singh, D. J.; Krakauer, H.; Haas, C.; Pickett, W. E. Theoretical determination that electrons act as anions in the electride Cs^+(15-crown-5)$_2$ e^-. *Nature* **1993**, *365*, 39−42.
(73) Toda, Y.; Kubota, Y.; Hirano, M.; Hirayama, H.; Hosono, H. Surface of Room-Temperature-Stable Electride $[Ca_{24}Al_{28}O_{64}]^{4+}(4e^-)$: Preparation and Its Characterization by Atomic-Resolution Scanning Tunneling Microscopy. *ACS Nano* **2011**, *5*, 1907−1914.
(74) Silvi, B.; Savin, A. Classification of chemical bonds based on topological analysis of electron localization function. *Nature* **1994**, *371*, 683−686.
(75) Matito, E.; Silvi, B.; Duran, M.; Solà, M. Electron localization function at the correlated level. *J. Chem. Phys.* **2006**, *125*, 024301.
(76) Johnson, E. R.; Keinan, S.; Mori-Sánchez, P.; Contreras-García, J.; Cohen, A. J.; Yang, W. Revealing noncovalent interactions. *J. Am. Chem. Soc.* **2010**, *132*, 6498−6506.
(77) Contreras-García, J.; Johnson, E. R.; Keinan, S.; Chaudret, R.; Piquemal, J.-P.; Beratan, D. N.; Yang, W. NCIPLOT: a program for plotting noncovalent interaction regions. *J. Chem. Theory Comput.* **2011**, *7*, 625−632.
(78) Schmider, H. L.; Becke, A. D. Chemical content of the kinetic energy density. *J. Mol. Struct.: THEOCHEM* **2000**, *527*, 51−61.
(79) Bader, R. F. W. *Atoms in Molecules: A Quantum Theory*; Oxford University Press: Oxford, U.K., 1990.
(80) Dale, S. G.; Otero-de-la Roza, A.; Johnson, E. R. Density-functional description of electrides. *Phys. Chem. Chem. Phys.* **2014**, *16*, 14584−14593.
(81) Burke, K.; Perdew, J. P.; Levy, M. Improving energies by using exact electron densities. *Phys. Rev. A: At., Mol., Opt. Phys.* **1996**, *53*, R2915.
(82) Sancho-García, J.; Pérez-Jiménez, A. Improved accuracy with medium cost computational methods for the evaluation of bond length alternation of increasingly long oligoacetylenes. *Phys. Chem. Chem. Phys.* **2007**, *9*, 5874−5879.
(83) Casademont-Reig, I.; Woller, T.; Contreras-García, J.; Alonso, M.; Torrent-Sucarrat, M.; Matito, E. New electron delocalization tools to describe the aromaticity in porphyrinoids. *Phys. Chem. Chem. Phys.* **2018**, *20*, 2787−2796.
(84) Casademont-Reig, I.; Ramos-Cordoba, E.; Torrent-Sucarrat, M.; Matito, E. Aromaticity descriptors based on electron delocalization. *Aromaticity Modern Computational Methods and Applications* **2021**.
(85) Casademont-Reig, I.; Ramos-Cordoba, E.; Torrent-Sucarrat, M.; Matito, E. Aromaticity descriptors based on electron delocalization; In *Aromaticity Modern Computational Methods and Applications*; Fernández, I., Ed.; Elsevier: Amsterdam, Netherlands, 2021.
(86) Torrent-Sucarrat, M.; Navarro, S.; Cossío, F. P.; Anglada, J. M.; Luis, J. M. Relevance of the DFT method to study expanded porphyrins with different topologies. *J. Comput. Chem.* **2017**, *38*, 2819−2828.
(87) Chen, W.; Li, Z.-R.; Wu, D.; Li, Y.; Sun, C.-C.; Gu, F. L.; Aoki, Y. Nonlinear optical properties of alkalides Li^+(calix[4] pyrrole) M^-(M= Li, Na, and K): Alkali anion atomic number dependence. *J. Am. Chem. Soc.* **2006**, *128*, 1072−1073.
(88) Das, P.; Saha, R.; Chattaraj, P. K. Encapsulation of Mg_2 inside aC_{60} cage forms an electride. *J. Comput. Chem.* **2020**, *41*, 1645−1653.
(89) Li, Z.-J.; Wang, F.-F.; Li, Z.-R.; Xu, H.-L.; Huang, X.-R.; Wu, D.; Chen, W.; Yu, G.-T.; Gu, F. L.; Aoki, Y. Large static first and second hyperpolarizabilities dominated by excess electron transition for radical ion pair salts $M_2^{\cdot+}$ $TCNQ^{\cdot-}$(M= Li, Na, K). *Phys. Chem. Chem. Phys.* **2009**, *11*, 402−408.
(90) Salehi, N.; Vessally, E.; Edjlali, L.; Alkorta, I.; Es' haghi, M. The investigation of cavity-trapped electrons in the Na_n@Tetracyanoethylene (n = 1−4) systems. *Chem. Rev. Lett.* **2020**, *3*, 207−212.
(91) Saha, R.; Chattaraj, P. K. Activation of small molecules (H_2, CO_2, N_2O, CH_4, and C_6H_6) by a porphyrinoid-based dimagnesium (I) complex, an electride. *ACS omega* **2018**, *3*, 17199−17211.
(92) Wang, Y.-F.; Li, Z.-R.; Wu, D.; Sun, C.-C.; Gu, F.-L. Excess electron is trapped in a large single molecular cage $C_{60}F_{60}$. *J. Comput. Chem.* **2010**, *31*, 195−203.
(93) Yanai, T.; Tew, D. P.; Handy, N. C. A new hybrid exchange−correlation functional using the Coulomb-attenuating method (CAM-B3LYP). *Chem. Phys. Lett.* **2004**, *393*, 51−57.
(94) Zheng, J.; Xu, X.; Truhlar, D. G. Minimally augmented Karlsruhe basis sets. *Theor. Chem. Acc.* **2011**, *128*, 295−305.
(95) Casademont-Reig, I.; Ramos-Cordoba, E.; Torrent-Sucarrat, M.; Matito, E. How aromatic are molecular nanorings? The case of a six-porphyrin nanoring. *ChemRxiv*, February 16, 2021, ver. 1. DOI: 10.26434/chemrxiv.14035919.v1 (accessed 2021-05-12).
(96) Becke, A. D. Density-functional thermochemistry. III. The role of exact exchange. *J. Chem. Phys.* **1993**, *98*, 5648−5652.
(97) Stephens, P. J.; Devlin, F. J.; Chabalowski, C. F.; Frisch, M. J. Ab initio calculation of vibrational absorption and circular dichroism spectra using density functional force fields. *J. Phys. Chem.* **1994**, *98*, 11623−11627.
(98) Zhao, Y.; Truhlar, D. G. The M06 suite of density functionals for main group thermochemistry, thermochemical kinetics, noncovalent interactions, excited states, and transition elements: two new functionals and systematic testing of four M06-class functionals and 12 other functionals. *Theor. Chem. Acc.* **2008**, *120*, 215−241.
(99) Yu, H. S.; He, X.; Li, S. L.; Truhlar, D. G. MN15: A Kohn−Sham global-hybrid exchange−correlation density functional with broad accuracy for multi-reference and single-reference systems and noncovalent interactions. *Chem. Sci.* **2016**, *7*, 5032−5051.
(100) Møller, C.; Plesset, M. S. Note on an approximation treatment for many-electron systems. *Phys. Rev.* **1934**, *46*, 618.

(101) Lee, T. J.; Taylor, P. R. A Diagnostic for Determining the Quality of Single-Reference Electron Correlation Methods. *Int. J. Quantum Chem.* **1989**, *36*, 199−207.
(102) Lee, T. J. Comparison of the T1 and D1 diagnostics for electronic structure theory: a new definition for the open-shell D1 diagnostic. *Chem. Phys. Lett.* **2003**, *372*, 362−367.
(103) Ramos-Cordoba, E.; Salvador, P.; Matito, E. Separation of dynamic and nondynamic correlation. *Phys. Chem. Chem. Phys.* **2016**, *18*, 24015−24023.
(104) Ramos-Cordoba, E.; Matito, E. Local Descriptors of dynamic and nondynamic correlation. *J. Chem. Theory Comput.* **2017**, *13*, 2705−2711.
(105) Via-Nadal, M.; Rodríguez-Mayorga, M.; Ramos-Cordoba, E.; Matito, E. Singling out weak and strong correlation. *J. Phys. Chem. Lett.* **2019**, *10*, 4032−4037.
(106) Via-Nadal, M.; Rodríguez-Mayorga, M.; Ramos-Cordoba, E.; Matito, E. *Range separation of the Coulomb hole*. Submitted for publication.
(107) Löwdin, P.-O. Quantum theory of many-particle systems. I. Physical interpretations by means of density matrices, natural spin-orbitals, and convergence problems in the method of configurational interaction. *Phys. Rev.* **1955**, *97*, 1474−1489.
(108) Smith, V. H., Jr Approximate natural orbitals for carbon 1 S. *Theor. Chim. Acta (Berlin)* **1967**, *7*, 245.
(109) Frisch, M. J.; Trucks, G. W.; Schlegel, H. B.; Scuseria, G. E.; Robb, M. A.; Cheeseman, J. R.; Scalmani, G.; Barone, V.; Petersson, G. A.; Nakatsuji, H.; et al. *Gaussian 16* Rev. C.01. 2016; Gaussian Inc. Wallingford, CT.
(110) Stanton, J. F.; Gauss, J.; Cheng, L.; Harding, M. E.; Matthews, D. A.; Szalay, P. G. *CFOUR, Coupled-Cluster techniques for Computational Chemistry, a quantum-chemical program package*. With contributions from Auer, A. A.; Bartlett, R. J.; Benedikt, U.; Berger, C.; Bernholdt, D. E.; Blaschke, S.; Bomble, Y. J.; Burger, S.; Christiansen, O.; Datta, D.; Engel, F.; Faber, R.; Greiner, J.; Heckert, M.; Heun, O.; Hilgenberg, M.; Huber, C.; Jagau, T.-C.; Jonsson, D.; Jusélius, J.; Kirsch, T.; Klein, K.; Kopper, G. M.; Lauderdale, W. J.; Lipparini, F.; Metzroth, T.; Mück, L. A., O'Neill, D. P.; Nottoli, T.; Price, D.R.; Prochnow, E.; Puzzarini, C.; Ruud, K.; Schiffmann, F.; Schwalbach, W.; Simmons, C.; Stopkowicz, S.; Tajti, A.; Vázquez, J., Wang, F.; Watts, J. D. and the integral packages MOLECULE (Almlöf, J.; Taylor, P. R.), PROPS (Taylor, P. R.), ABACUS (Helgaker, T.; Jensen, H. J. Aa., Jørgensen, P., Olsen, J.), and ECP routines by Mitin, A. V., van Wüllen, C.. For the current version, see http://www.cfour.de.
(111) Handy, N. C.; Schaefer, H. F., III On the evaluation of analytic energy derivatives for correlated wave functions. *J. Chem. Phys.* **1984**, *81*, 5031−5033.
(112) Müller, A. M. K. Explicit approximate expression between reduced two- and one-particle density matrices. *Phys. Lett. A* **1984**, *105A*, 446−452.
(113) Rodríguez-Mayorga, M.; Ramos-Cordoba, E.; Via-Nadal, M.; Piris, M.; Matito, E. Comprehensive benchmarking of density matrix functional approximations. *Phys. Chem. Chem. Phys.* **2017**, *19*, 24029−24041.
(114) Cioslowski, J.; Piris, M.; Matito, E. Robust validation of approximate 1-matrix functionals with few-electron harmonium atoms. *J. Chem. Phys.* **2015**, *143*, 214101.
(115) Rodríguez-Mayorga, M.; Ramos-Cordoba, E.; Feixas, F.; Matito, E. Electron correlation effects in third-order densities. *Phys. Chem. Chem. Phys.* **2017**, *19*, 4522−4529.
(116) Feixas, F.; Matito, E.; Duran, M.; Solà, M.; Silvi, B. Electron localization function at the correlated level: a natural orbital formulation. *J. Chem. Theory Comput.* **2010**, *6*, 2736−2742.
(117) Ruiz, I.; Matito, E.; Holguín-Gallego, F. J.; Francisco, E.; Pendás, Á. M.; Rocha-Rinza, T. Fermi and Coulomb correlation effects upon the interacting quantum atoms energy partition. *Theor. Chem. Acc.* **2016**, *135*, 209.
(118) Matito, E.; Solà, M.; Salvador, P.; Duran, M. Electron sharing indexes at the correlated level. Application to aromaticity calculations. *Faraday Discuss.* **2007**, *135*, 325−345.
(119) Feixas, F.; Solà, M.; Barroso, J. M.; Ugalde, J. M.; Matito, E. New Approximation to the Third-Order Density. Application to the Calculation of Correlated Multicenter Indices. *J. Chem. Theory Comput.* **2014**, *10*, 3055−3065.
(120) Keith, T. A. *AIMAll*, Ver. 14.11.23; TK Gristmill Software, Overland Park KS, 2014; aim.tkgristmill.com).
(121) Pendás, A. M.; Blanco, M. A.; Costales, A.; Sánchez, P. M.; Luaña, V. Non-nuclear maxima of the electron density. *Phys. Rev. Lett.* **1999**, *83*, 1930−1933.
(122) Fradera, X.; Austen, M. A.; Bader, R. F. W. The Lewis model and beyond. *J. Phys. Chem. A* **1999**, *103*, 304−314.
(123) Ramos-Cordoba, E.; Postils, V.; Salvador, P. Oxidation states from wave function analysis. *J. Chem. Theory Comput.* **2015**, *11*, 1501−1508.
(124) Postils, V.; Delgado-Alonso, C.; Luis, J. M.; Salvador, P. An objective alternative to IUPAC's approach to assign oxidation states. *Angew. Chem.* **2018**, *130*, 10685−10689.
(125) Min, X.; Popov, I. A.; Pan, F.-X.; Li, L.-J.; Matito, E.; Sun, Z.-M.; Wang, L.-S.; Boldyrev, A. I. All-metal antiaromaticity in Sb_4-type lanthanocene anions. *Angew. Chem., Int. Ed.* **2016**, *55*, 5531−5535.
(126) Grande-Aztatzi, R.; Mercero, J. M.; Matito, E.; Frenking, G.; Ugalde, J. M. The aromaticity of dicupra [10]annulenes. *Phys. Chem. Chem. Phys.* **2017**, *19*, 9669−9675.
(127) Postils, V.; Rodríguez, M.; Sabenya, G.; Conde, A.; Díaz-Requejo, M. M.; Pérez, P. J.; Costas, M.; Solà, M.; Luis, J. M. Mechanism of the selective Fe-catalyzed arene carbon−hydrogen bond functionalization. *ACS Catal.* **2018**, *8*, 4313−4322.
(128) Gimferrer, M.; Van der Mynsbrugge, J.; Bell, A. T.; Salvador, P.; Head-Gordon, M. Facing the challenges of borderline oxidation state assignments using state-of-the-art computational methods. *Inorg. Chem.* **2020**, *59*, 15410−15420.
(129) Ampßler, T.; Monsch, G.; Popp, J.; Riggenmann, T.; Salvador, P.; Schröder, D.; Klüfers, P. Not guilty on every count: The "non-innocent" nitrosyl ligand in the framework of IUPAC's oxidation-state formalism. *Angew. Chem., Int. Ed.* **2020**, *59*, 12381−12386.
(130) Salvador, P.; Ramos-Cordoba, E. *APOST-3D program*; Universitat de Girona: Girona, Spain, 2012.
(131) Martín Pendás, A.; Francisco, E.; Blanco, M. A. An electron number distribution view of chemical bonds in real space. *Phys. Chem. Chem. Phys.* **2007**, *9*, 1087−1092.
(132) Cancés, E.; Keriven, R.; Lodier, F.; Savin, A. How electrons guard the space: shape optimization with probability distribution criteria. *Theor. Chem. Acc.* **2004**, *111*, 373−380.
(133) Bader, R. F. W.; Stephens, M. E. Fluctuation and correlation of electrons in molecular systems. *Chem. Phys. Lett.* **1974**, *26*, 445−449.
(134) Bader, R. F. W.; Stephens, M. E. Spatial localization of the electronic pair and number distributions in molecules. *J. Am. Chem. Soc.* **1975**, *97*, 7391−7399.
(135) Chalvet, O.; Daudel, R.; Diner, S.; Malrieu, J. P. *Localization and Delocalization in quantum Chemistry*; Reidel: Dordrecht, The Netherlands, 1975; Vol. *I*.
(136) Chalvet, O.; Daudel, R.; Diner, S.; Malrieu, J. P. *Localization and Delocalization in quantum Chemistry*; Reidel: Dordrecht, The Netherlands, 1976; Vol. *II*.
(137) Francisco, E.; Martín Pendás, A.; Blanco, M. A. Electron number probability distributions for correlated wave functions. *J. Chem. Phys.* **2007**, *126*, 094102.
(138) Francisco, E.; Pendás, A. M.; Blanco, M. A. EDF: Computing electron number probability distribution functions in real space from molecular wave functions. *Comput. Phys. Commun.* **2008**, *178*, 621−634.
(139) Pendás, A. M.; Francisco, E. Chemical bonding from the statistics of the electron distribution. *ChemPhysChem* **2019**, *20*, 2722−2741.

(140) Martín Pendás, Á.; Francisco, E. Local spin and open quantum systems: clarifying misconceptions, unifying approaches. *Phys. Chem. Chem. Phys.* **2021**, *23*, 8375−8392.
(141) Ramos-Cordoba, E.; Matito, E.; Mayer, I.; Salvador, P. Toward a unique definition of the local spin. *J. Chem. Theory Comput.* **2012**, *8*, 1270−1279.
(142) Ramos-Cordoba, E.; Matito, E.; Salvador, P.; Mayer, I. Local spins: improved Hilbert-space analysis. *Phys. Chem. Chem. Phys.* **2012**, *14*, 15291−15298.